Citation
Zhang, X. and Hao, H. 2019. Improved impact resistant capacity of segmental column with fibre reinforced polymer wrap. International Journal of Impact Engineering. 125: pp. 117-133. http://doi.org/10.1016/j.ijimpeng.2018.11.009

Improved Impact Resistant Capacity of Segmental Column with Fibre Reinforced Polymer Wrap

Xihong Zhang[1], Hong Hao[1,2 *]

[1] Centre for Infrastructural Monitoring and Protection, School of Civil and Mechanical Engineering, Curtin University, Australia

[2] School of Civil Engineering, Guangzhou University, China

*Hong.hao@curtin.edu.au

Abstract

Our previous studies investigated the response of precast segmental columns subjected to lateral impact loading, and found that the columns exhibited better flexibility and impact resistance capability as compared to monolithic cast-in-place column. The damage and failure of segmental column were mainly due to flexural compression induced damages when subjected to mid-span impact, and concrete shear failure when subjected to near base impact. In this paper, we utilize FRP to wrap the concrete segments to improve its impact resistant capacity. Laboratory impact tests on scaled columns are conducted. The columns are impacted at mid-span, segmental joint near column base and directly onto the centre of the bottom concrete segment which are respectively associated with the flexural bending mode, combined bending and shear mode, and direct shear deformation mode. The responses of the columns are examined and compared with those non-retrofitted columns. Then, a detailed three-dimensional numerical model of the segmental column is generated and validated with lab test results. The numerical model can be used to calculate the responses of the segmental columns subjected to lateral impact loading for design analyses.

Keyword: Segmental column, impact, reinforced concrete, FRP, mitigation

1. Introduction

1.1 Background

Accelerated construction with precast segmental elements have attracted much attention recently. This is because it can greatly improve construction efficiency (up to 50% construction time [1]), ensure construction quality, minimize traffic disruption, and reduce environmental impact (minimum site work and no site casting). In addition, new materials such as ultra-high-performance concrete and fibre reinforced concrete which require heat curing and special mixing become feasible for precast segmental element.

According to the bonding type of prestress system, segmental columns can be categorized into bonded or unbonded prestress system. With unbonded post-tensioning prestress system, a segmental column is erected on site and then the tendon is post-tensioned. Such system exhibits outstanding self-centring capacity because the post-tensioned tendon could bring the deformed column back to its original position. However, because of the gap between adjacent concrete segments, the unbonded tendon is vulnerable to corrosion damage [2-4]. For segmental column with bonded prestress system, the preserved duct for prestress tendon is grouted with cementitious materials after the tendon is stressed. The bonded prestress system has been found to increase column lateral strength, and is capable of dissipating more energy because of the yielding of the bonded tendon when the column is laterally loaded. Nevertheless, the yielding of tendon reduces the self-centring capacity of the column [5, 6].

There are very limited studies available in the literature about the impact resistant capacity of segmental column while most previous studies concentrated on the earthquake resistance performance of segmental columns [7-10]. Recently Zhang et al. [11, 12] conducted pendulum impact tests on precast segmental column with unbonded prestress tendon. By comparing with conventional monolithic column, it was found that when subjected to mid-span impact, segmental column exhibited more flexural deformation capacity and better self-centring ability after the impact. Since the segmental columns was more flexible under impact loading, lower peak impact loads were resulted and measured when subjected to lateral impacts of the same impactor weight and velocity. When impacted at different locations along the segmental columns, different responses

and failure modes would be excited. For instance, when impacted at mid-span of the segmental column the column developed substantial flexural bending deformation. When impacted at segmental joint near column base, combined flexural bending and shear deformation mode was resulted because the moment resistant capacity at segmental joint was low. When the column was impacted directly on the bottom segment, shear dominated failure was observed, where segmental joint opening was not observed to the segmental column. It was also found that friction between adjacent segments was not sufficient to resist shear slippage at the segment joint under lateral impacts. To improve segmental shear resistance, trapezoidal prism shape shear key made of concrete which is commonly used for precast concrete elements was introduced. Impact test on segmental columns with shear key found that because of the sudden change in segment geometry around the concrete tenon and mortise, more severe crushing damages to concrete segments especially around the shear key were observed due to stress concentration [13]. To relief column damage due to stress concentration around shear key, Zhang et al. optimised the concrete shear key with curved dome-shape [14]. Validation test proved less concrete damage with the improved domed shear key.

Mitigation retrofit for segmental column against impact loading is not available in literature. Existing retrofitting methods on segmental columns are primarily against earthquake loading. For instance, Chou and Chen [4] installed energy dissipation device to the column-footing joint. Ou et al. [8, 9, 15] employed energy dissipation bars at segmental joints. Both mild steel and shape-memory-alloy were adopted. Motaref et al. [16] used CFRP at segmental joints to reduce damage. Since the responses of segmental columns under earthquake loading and impact loading are fundamentally different, the effectiveness and efficiency of these methods in protecting segmental columns under earthquake ground motions are not necessarily the same when the column is subjected to lateral impacts. For conventional monolithic RC columns, FRP has been commonly utilized to improve column impact resistance capacity. To apply FRP wrap around the column was found to be able to provide substantial confinement and therefore increase the compressive strength of concrete and the column [17, 18], comparable to applying confinement by steel reinforcement. Previous testing results showed noticeable increase in concrete compressive strength [19].

1.2 FRP confinement model

The confinement of concrete using FRP is based on a well-established mechanism that the lateral expansion of concrete column is resisted by the FRP wrap which provides a confining pressure to the concrete. FRP wrap ruptures if the tensile stress in the hoop direction is exceeded. Many studies have been made to investigate and model the behavior of concrete in FRP-confined rectangular columns [20-24], leading to different models, of which ACI-440 [25] model is one of the most commonly utilized in predicting FRP confined concrete properties.

The compressive strength of FRP-confined concrete fc' is closely related to the effective confining pressure f_1' by the FRP wrap, which is defined as

$$f_1' = k_s f_1 \tag{1}$$

where k_s is the shape factor to account for the effect of non-uniform confinement, and f_1 is the equivalent confining pressure by the FRP wrap to an equivalent circular column, which can be evaluated by the following equation:

$$f_1 = \frac{2E_{frp}\varepsilon_j t}{D} \tag{2}$$

where ε_j is the nominal hoop rupture strain in the FRP, and D is the equivalent diameter of the column. E_{frp} and t are the elastic modulus and total thickness of the FRP.

In ACI-440 [25], the shape factor is defined as the ratio of the effective confinement area to the total area of concrete.

$$k_s = \frac{A_e}{A_g} = \frac{1 - \left((b - 2R_c)^2 + (h - 2R_c)^2/3A_g\right) - \rho_{sc}}{1 - \rho_{sc}} \tag{3}$$

where A_e and A_g are the effective and gross areas of the column; R_c is the radius of the corner and ρ_{sc} is the longitudinal reinforcement ratio. The equivalent diameter of the rectangular column $D = \frac{2bh}{b+h}$, where b and h are the width and depth of the cross-section of the column. The compressive strength of the confined concrete can be predicted using Mander's [26] equation as

$$\frac{f_{cc}'}{f_{co}'} = 2.254\sqrt{1 + 7.94 f_1'/f_{co}'} - \frac{2f_1'}{f_{co}'} - 1.254 \quad (4)$$

where f_{cc}' is the FRP-confined concrete strength, and f_{co}' is the unconfined uniaxial compressive strength of the concrete. With the column and FRP design inputs, the confined concrete strength with FRP wrap can then be calculated.

1.3 Aim and scope of this study

Since the damage to the segmental column is primarily due to the damage of concrete especially due to excessive flexural induced compression and shear damages, mitigation retrofit is provided by applying fibre reinforced polymer wraps to the concrete segment which could provide confinement to improve concrete strength. Lateral impact tests and numerical simulations are conducted on segmental columns wrapped with FRP. Columns are impacted at mid-span, bottom segmental joint and base segment. Comparison with non-retrofitted segmental columns was also made to evaluate the effectiveness of the FRP retrofitting.

2. Experimental Examination

2.1 Column design

Figure 1 shows the schematic view of the segmental column. Scaled columns of 800mm tall with 100mm by 100mm squared cross-section are designed. The designated dimension represents ¼ scale model of 3.2m tall column. Each column comprises of 5 reinforced concrete segments (Figure 1b). ϕ6mm deformed bars are used as longitudinal reinforcement, and ϕ4mm plain bars are used as transverse reinforcement at 40mm spacing. To improve segmental shear resistance and to reduce stress concentration at shear key, dome-shape concrete shear key is designed. The bottom segment is cast independently and then connected to the concrete footing with two ϕ6mm starter bars and concrete shear key. The footing is 400mm by 400mm by 140mm, which is fully fixed to the strong floor with post-tensioning bolts. The columns are free-standing with a concrete cube and a series of steel plates stacked on top of the column (total weight of 288kg).

The concrete segments are integrated with the footing and top mass with post-tensioning tendon. A ϕ9.3mm 7-wire super-strand is pulled through the centre of the segments with 30kN post-tensioning force (about 8.5% of the column axial compressive capacity). The uniaxial compressive strength of concrete is 34MPa and the flexural bending strength is 5MPa. The density of the longitudinal and transverse reinforcements is 7800kg/m^3 and the yield strengths are 500MPa and 300MPa respectively. The Young's modulus of the reinforcement is 200GPa. The density, proof strength and Young's modulus of the prestress tendon are 7850kg/m^3, 1860MPa and 195GPa, respectively. The four corners of each concrete segment are rounded (r10mm). Two layers of Basalt fibre reinforced polymer (BFRP) are glued to wrap each segment. The thickness of BFRP is 0.12mm per layer. The density is 2500kg/m^3, and the characteristic static tensile strength is 1640MPa and Young's modulus is 77.9GPa. Reference [27] lists the detailed mechanical properties of the BFRP utilized in the test. Sikadur®-300 is applied as epoxy whose tensile strength is 45MPa and tensile modulus of elasticity is 3500MPa (7 days at room temperature).

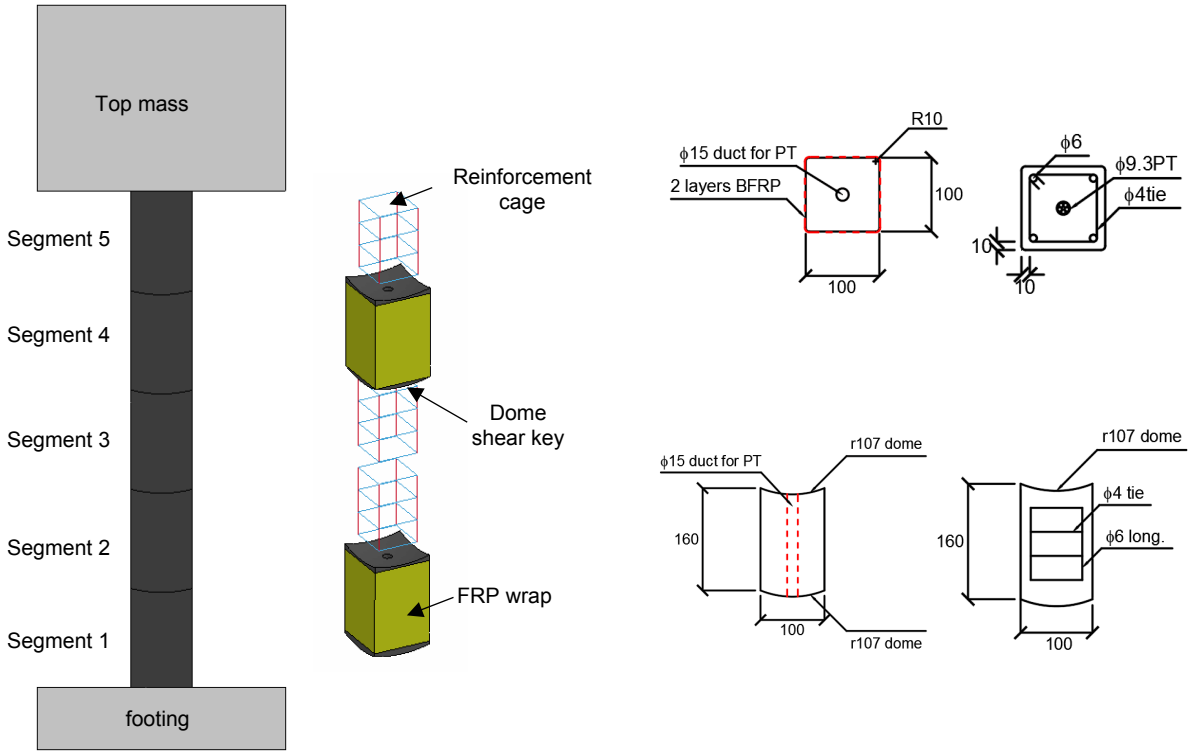

Figure 1 Illustration of segmental column design

2.2 Test system

A pendulum impact system is used for the impact test. The impactor is made of 300kg solid steel block hinged with a 2.8m long pendulum arm. In each test, the impactor is lifted to the design angle and then released to generate impact onto the column at different impact velocities. The impactor is then pulled back manually to avoid impacting the column for a second time. To strike at different locations of the column, the columns are elevated by inserting precast reinforced concrete slabs underneath the footing.

A load cell is installed in front of the impactor to measure the impact load. Linear voltage displacement transducers (LVDTs) are installed behind the column at different locations to monitor column lateral displacement. The sensors are connected to a data acquisition system and logged at 50 kHz frequency. A high-speed camera is setup to video the entire deformation-to-failure process of the column. With the aid of tracking matrix glued to the centre of each concrete segment, the high-speed video images were post-processed with digital image correlation technique to derive the segment displacement time histories.

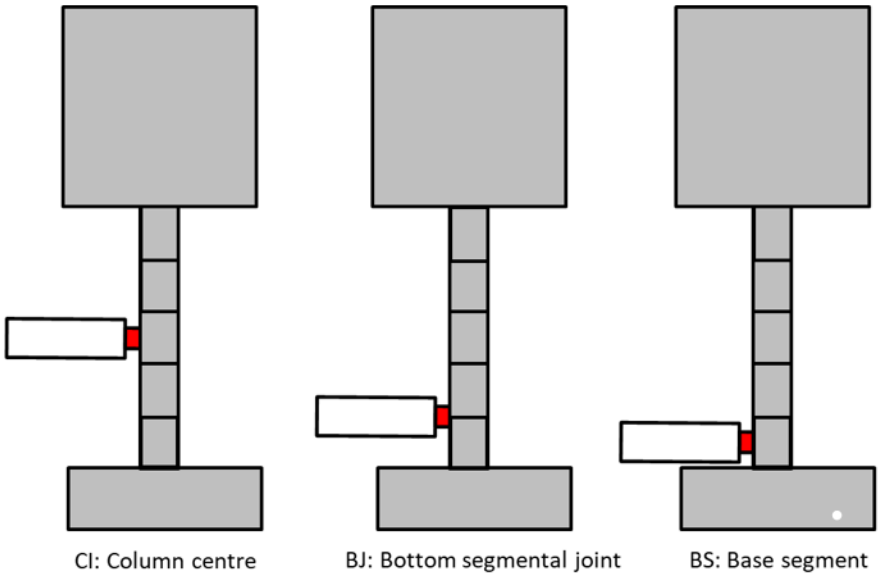

Figure 2 Schematic view of the impact locations onto the segmental columns

Column	Impact location	Mitigation	Impact No.	Est. velocity (m/s)
S5KD-CI[14]	Mid-span	-	Impact 01	0.23
			Impact 02	0.64
			Impact 03	1.37
			Impact 04	2.71
			Impact 05	3.59
S5KD-BJ[14]	Base joint	-	Impact 01	0.23
			Impact 02	0.64
			Impact 03	1.37
			Impact 04	2.71
			Impact 05	3.59
S5KD-BS[14]	Base segment	-	Impact 01	0.23
			Impact 02	0.64
			Impact 03	1.37
			Impact 04	2.71
			Impact 05	3.59
S5KD-FRP-CI	Mid-span	FRP wrap	Impact 01	0.23
			Impact 02	0.64
			Impact 03	1.37
			Impact 04	2.71
			Impact 05	3.59
			Impact 06	4.05
S5KD-FRP-BJ	Base joint	FRP wrap	Impact 01	0.23
			Impact 02	0.64
			Impact 03	1.37
			Impact 04	2.71
			Impact 05	3.59
			Impact 06	4.05
			Impact 07	4.47
S5KD-FRP-BS	Base segment	FRP wrap	Impact 01	0.23
			Impact 02	0.64
			Impact 03	1.37
			Impact 04	2.71
			Impact 05	3.59

Table 1 Summary of test plan

2.3 Test scheme

To evaluate the effectiveness of FRP wrap for different response modes of segmental columns, the columns are impacted at mid-span, bottom segmental joint and centre of bottom segment (Figure 2), which correspond to the maximum flexural deformation, combined flexural bending and shear deformation, and direct shear failure mode when the columns are not retrofitted in the previous study [14]. Each column is subjected to

multiple impacts with gradually increased impact velocities, i.e. 0.23m/s, 0.67m/s, 1.38m/s, 2.74m/s, 3.62m/s, 4.05m/s and 4.47m/s, until total column failure. For comparison, the results from the same segmental columns without FRP wraps reported in a previous study [14] are also briefly discussed here. Table 1 summarizes the testing scheme, where S5KD-FRP represents segmental column with five segments and wrapped with FRP. CI, BJ and BS stand for impacted at centre of column (mid-span), bottom segmental joint and centre of bottom segment, respectively.

3. Results

Testing results for the three types of FRP retrofitted segmental columns under lateral impacts at different locations are presented in this section, which include column deformation-to-failure processes recorded with a high-speed camera, column damage and failure modes, impact load time histories and column lateral displacement time histories. Comparisons between the non-retrofitted and FRP-retrofitted columns are made to assess the effectiveness of FRP wrap in improving the column impact resistant capacity.

3.1 Impact at column mid-span

3.1.1 Deformation-to-failure process

Figure 3 shows the column response when impacted at mid-span of the column. Since in Impact 01, 02 and 03 the impact loads are relatively small which generated insignificant column responses, the high-speed camera images are therefore not presented. As shown, in Impact 04 (2.71m/s) when the impactor strikes on the mid-span of column S5KD-FRP-CI, it forces the column to deform sideway. Local deformation mode with large central deflection is excited at t=30ms. The maximum deformation of the column gradually moves from the centre of the column upwards to the top of the column (t=69ms), i.e., the response mode of the column transforms from localized deformation mode into global response mode during free vibration phase (t=389ms). As impact velocity increases to 3.59m/s (Impact 05), larger deflection of the column with apparent joint openings between the Segment 2 and 3 at t=20ms, and between Segment 3 and 4 at t=85ms are observed. Because of excessive flexural bending deformation, concrete compressive damage is resulted and can be observed in Segment 4. Despite very large deflection at the top of

the column during free vibration phase, the prestress tendon still manages to restore the deformed column. In the ultimate impact with velocity 4.05m/s, the column exhibits local deformation mode with large central deflection (t=20ms). Similar to that described above, the response mode of the column gradually changes. Because of substantial top deflection, the column eventually collapses due to overturn from the top of the column (t=598ms).

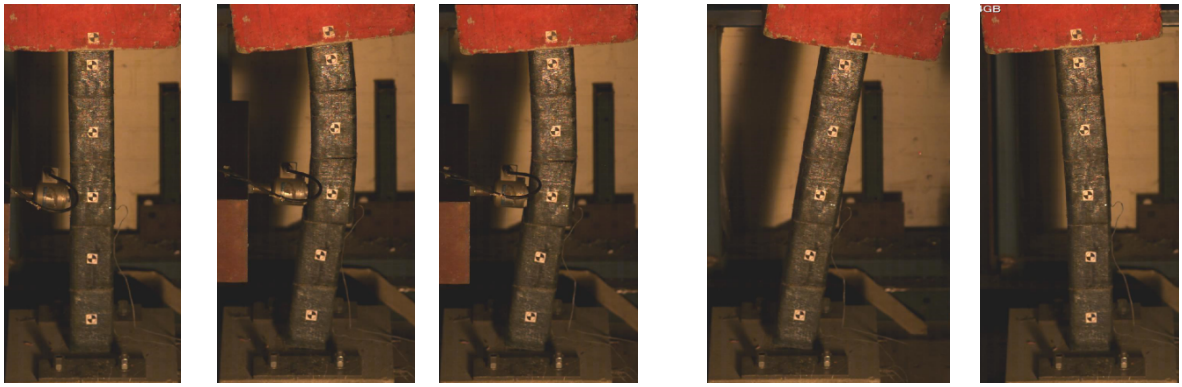

t=0ms t=30ms t=69ms t=389ms t=969ms

Impact 04

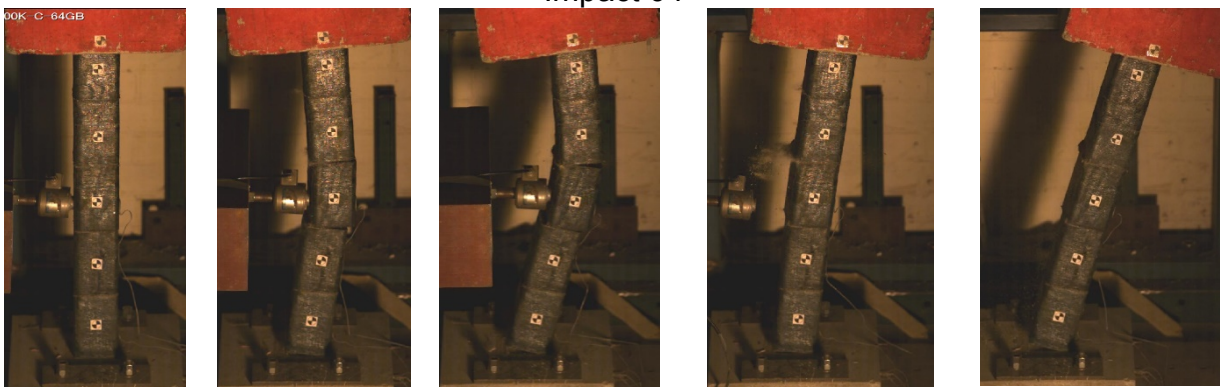

t=0ms t=20ms t=85ms t=178ms t=525ms

Impact 05

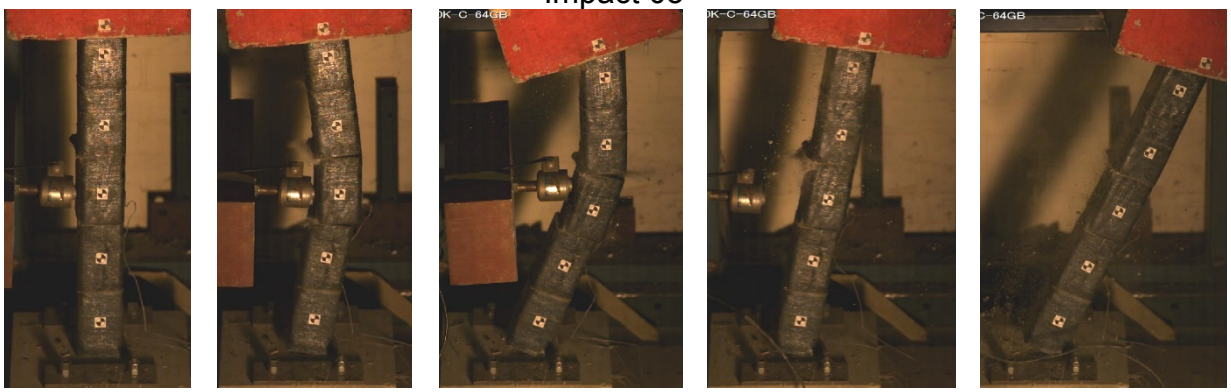

t=0ms t=20ms t=97ms t=246ms t=598ms

Impact 06

Figure 3 High-speed camera images of column S5KD-FRP-CI

3.1.2 Damage and failure of column

Figure 4 compares the damages and failure of the segmental columns with and without FRP retrofit. As can be observed, the non-retrofitted column experiences severe concrete segment damages especially to Segment 3 and 4 due to compressive damage induced by flexural bending. The column loses stability eventually under 3.59m/s impact as damages extend through neutral axis of column. In comparison, the retrofitted column is more resilient under mid-span impact. Most concrete segments remain intact under the lateral impacts. Only minor FRP rupture is formed to Segment 4 and the base segment, indicating substantial flexural compressive stress the concrete segments experience. The starter bars connecting the bottom segment and the footing snap as the column develops very large flexural bending deformation. The column collapses eventually because of excessive lateral displacement instead of severe column damage.

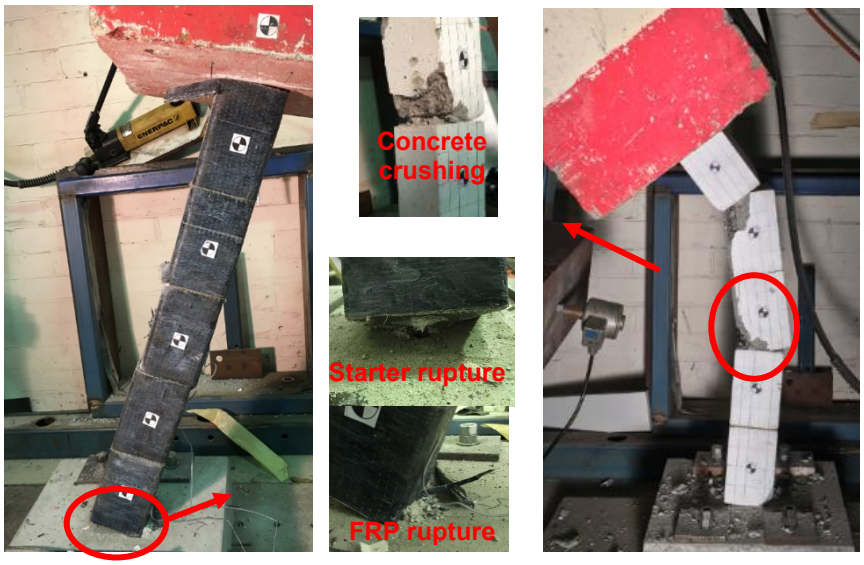

a) S5KD-FRP-CI b) S5KD-CI

Figure 4 Comparison of damage and failure of columns under mid-span impact a) FRP retrofitted column; b) Non-retrofitted column

3.1.3 Impact load time history

Figure 5a shows the impact load time histories recorded for column S5KD-FRP-CI. Because of malfunction of the loadcell, the impact loads for Impact 02, 03 and 04 were not properly recorded. As can be found, the impact loads for the mid-span impact on retrofitted segmental columns are featured with multiple peaks. An initial maximum impact loads are formed when the impactor strikes on the column. For instance, for Impact 01 an initial peak load of about 7.8kN is resulted upon the impactor strikes on the column, which then reduces to about 3kN but increases again to about 7kN reaching a 2nd peak on the load time history before it dissipates to ambient at about 28ms. As impactor velocity increases, larger impact load is resulted with longer duration acting on the segmental column. In Impact 05, an initial peak load of 21.5kN is measured followed which there are a few peaks until reduces to ambient at about 125ms. The featured multiple peaks on load time histories are due to the interaction between the impactor and the segmental column. In the ultimate 4.05m/s impact, a peak load of 23.6kN is resulted which dissipates to ambient at about 170ms.

Figure 5b compares the typical impact load time histories for the FRP-retrofitted and non-retrofitted columns. It can be found that under low-speed impact (0.23m/s in Impact 01), very similar initial peak loads are measured on the two columns because there are no damages caused to the columns. However, the 2nd peak load on the FRP wrapped column is larger than that on the non-retrofitted column but last for shorter duration due to higher column stiffness. When subjected to high-speed impact (4.05m/s in Impact 05), larger peak impact load (about 24kN) is resulted on column S5KD-CI than that on S5KD-FRP-CI (about 21.5kN). But the impactor acts on the latter column for longer duration owing to smaller column stiffness and larger deformation.

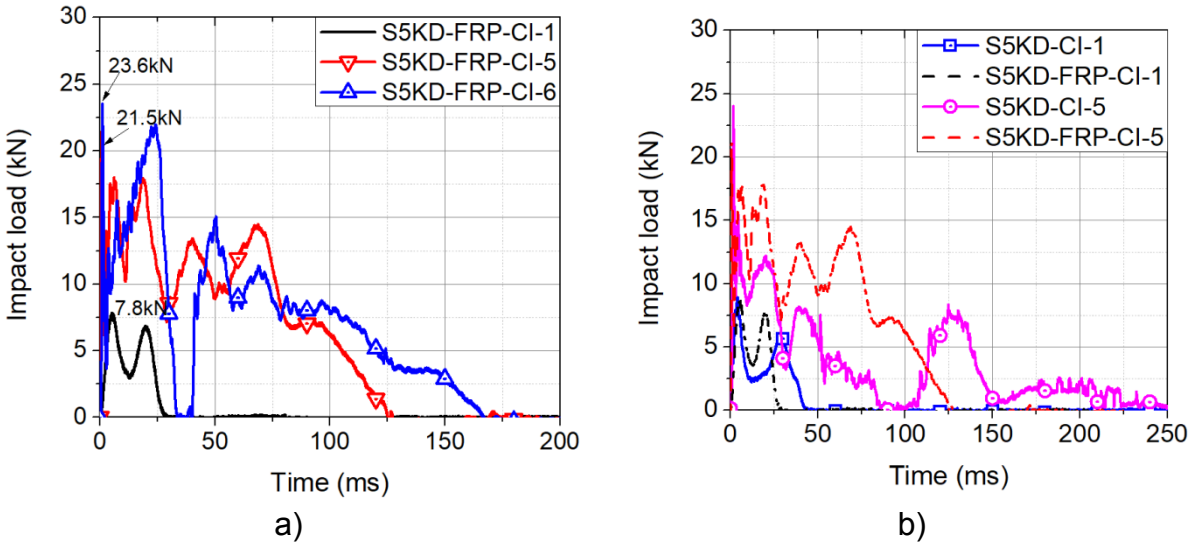

Figure 5 Impact load time histories for a) S5KD-FRP-CI; b) comparisons with S5KD-CI

3.1.4 Deflection time histories

Figure 6a shows the recorded column central deflection time history. As can be observed that an initial peak central deflection occurs during the forced vibration phase, which quickly rebounds and then forms a 2nd peak deflection during the free vibration phase. The column vibrates back and forth until it comes to rest. As the impact level increases, both the peak deflection and the vibration period increase. For instance, a peak deflection of 3.8mm is resulted at the centre of the column in Impact 01, which increases to 66.7mm in Impact 05. The associated column free vibration period also increases from 272ms to 820ms. This is because the larger impact force results in the segmental joint opening and damages the concrete segments. Figure 6b compares the central deflection time histories between the retrofitted and non-retrofitted columns. When subjected to low-velocity impact (0.23m/s), the responses of the two columns are very similar. The vibration amplitude of the FRP wrapped column is slightly lower than that of the non-retrofitted column. However, the difference becomes more apparent when the columns are subjected to high velocity impact (3.59m/s in Impact 04). A peak deflection of 66.3mm is measured at the centre of the FRP retrofitted column, which is 21% lower than that of the non-retrofitted column (84mm). Because of the FRP wrap and less damages to the concrete segments, the vibration period of the retrofitted column is also shorter than that of the non-retrofitted column.

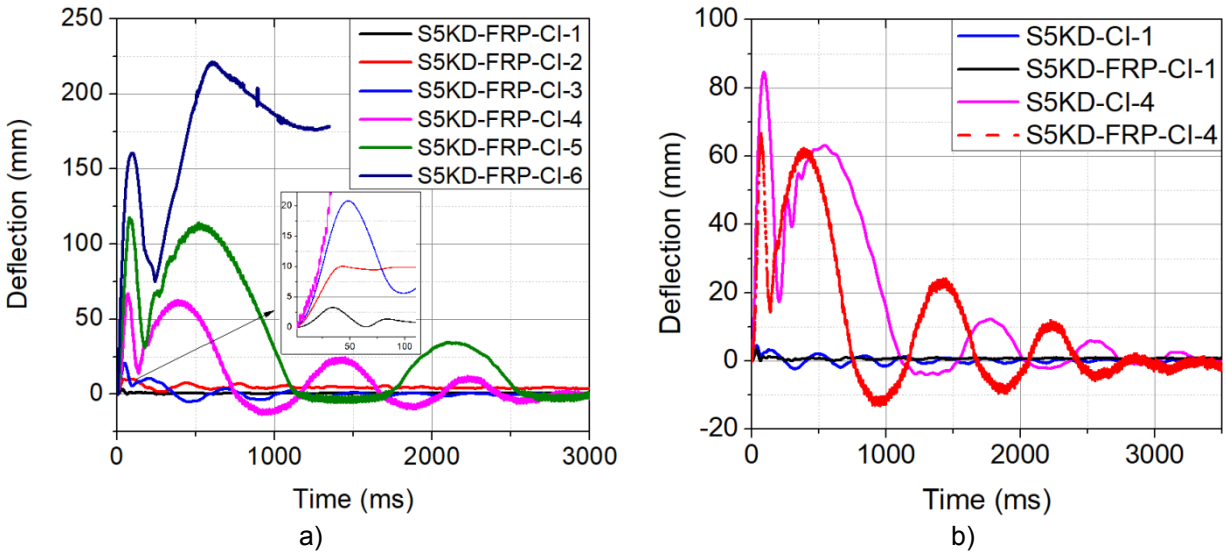

Figure 6 Deflection time histories at column mid-span for a) S5KD-FRP-CI; b) comparison with S5KD-CI

The peak and residual deflections at the top of the FRP retrofitted and non-retrofitted columns are summarized and compared in Figure 7a. Because the load cell did not record all the impact load time histories, impact velocity is utilized as the horizontal axis. As can be observed, the peak deflections of the retrofitted column are always smaller than those measured on the non-retrofitted columns. For instance, when impacted with 1.37m/s velocity in Impact 03, a peak deflection of 30.2mm is measured on S5KD-FRP-CI which is 24% lower than that of column S5KD-CI. When the columns are subjected to 3.59m/s impact in Impact 05, a peak deflection of the retrofitted column is 205.4mm while that of the non-retrofitted column is 258.6mm. As for the residual deflection, it can be found that negligible residual displacements are measured on the two columns when subjected to low velocity impacts in Impact 01 and 02. Column S5KD-CI inclines backwards after Impact 03 and 04 with residual displacements of -4.4mm and -4.8mm, respectively. In comparison, smaller residual deflections are measured on the FRP wrapped column. Residual top displacements are 1.6mm and -3.4mm after Impact 03 and 04. This is because with FRP wrapping the segments, much less concrete damages are resulted when the column is impacted.

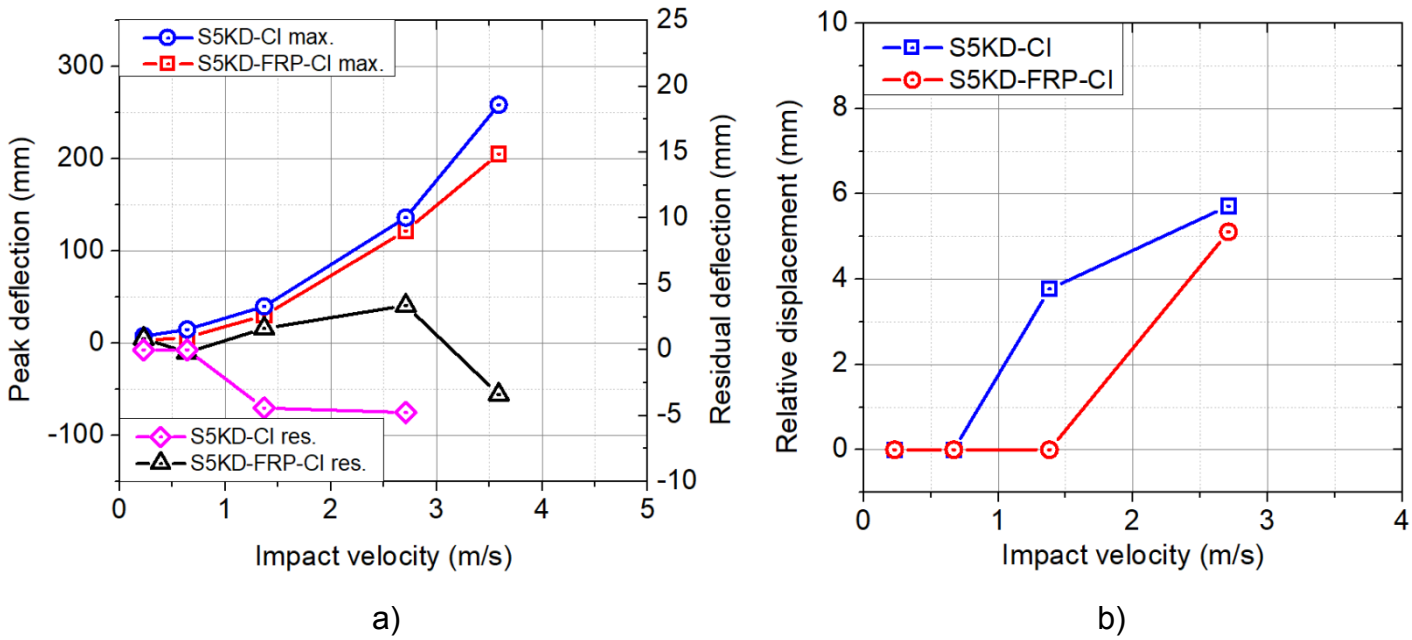

Figure 7 Comparisons of a) peak and residual deflections at column top; b) relative displacement

Segmental relative displacement is a major concern for segmental column under lateral impact. Figure 7b compares the relative displacements between Segment 2 and 3 for the two columns. Because the columns are impacted at the centre of Segment 3, maximum shear forces are resulted between these two segments. No relative displacements are found when the impact levels are relatively small. In Impact 03 (1.37m/s), a relative displacement of nearly 4mm is recorded on the non-retrofitted column, which further increases to almost 6mm in Impact 04. In comparison, no relative displacement is resulted on the retrofitted column after Impact 03. This is because no concrete damage occurs to the FRP wrapped column. However, because of large lateral force in Impact 04, over 5mm relative displacement is resulted at the joint between Segment 2 and 3, which nevertheless is still smaller than that of the non-retrofitted column.

3.2 Impact at bottom segmental joint

3.2.1 Deformation-to-failure process

When impacted at bottom segmental joint, segmental column exhibits different response from that described above, i.e. combined flexural bending and shear deformation mode [13]. Figure 8 depicts the responses when the column is wrapped with FRP. As shown, in Impact 05 impacting at the bottom segmental joint forces the joint to open (t=10ms). Flexural deformation occurs with the largest curvature developed near the column bottom at the impacted point. With higher impact velocity in Impact 06, larger segmental joint opening can be observed (t=10ms). The localized flexural deformation gradually transforms to the global response mode with the largest deformation occurring at the top end of the column (t=283ms). Similar response characteristics can be observed in Impact 07, but the high-speed impact causes larger responses and also indents on the FRP wrapped concrete segment. At t=26ms, the impactor pushes the column to bend with an excessive opening. As a result, the bottom concrete segment rotates substantially against the bottom right corner. Concrete crushing damage can be observed as a resulted of the excessive rotation at the joint (t=111ms).

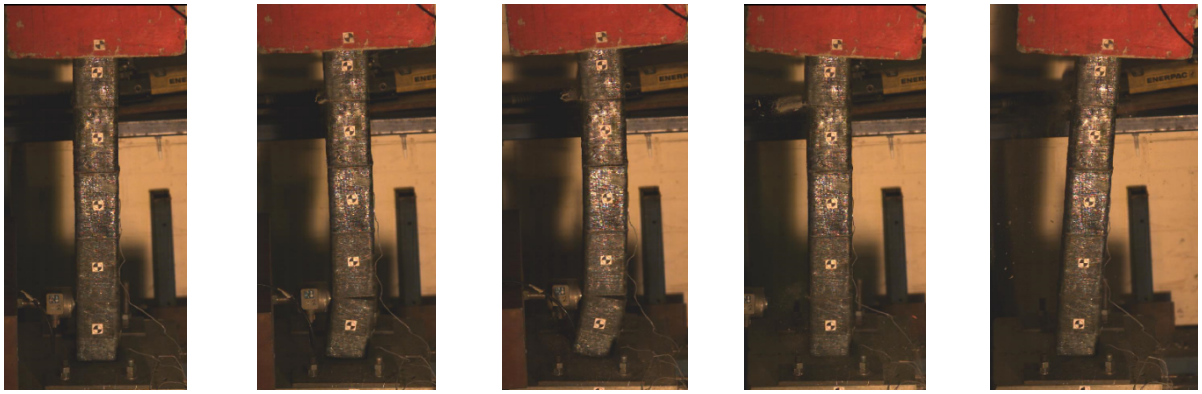

t=0ms t=10ms t=22ms t=99ms t=335ms

Impact 05

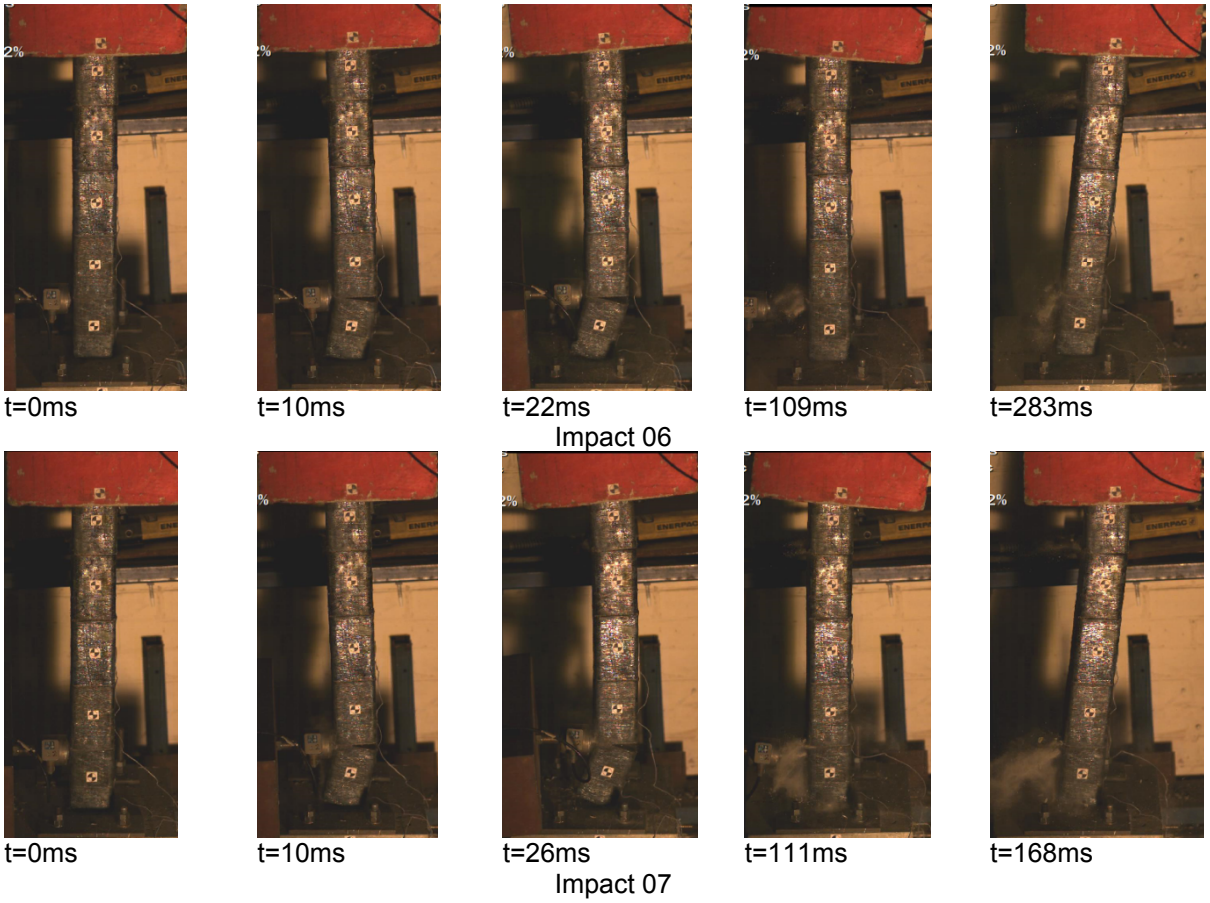

Figure 8 High-speed camera images of column S5KD-FRP-BJ in three impact tests

3.2.2 Damage and failure of the column

Figure 9 compares the damage and failure modes of the retrofitted and non-retrofitted segmental columns subjected to impact at the bottom segmental joint. As can be seen, severe damages to the two bottom segments of the non-retrofitted column S5KD-BJ occur. Flexural bending induced compressive stress leads to damages in the two bottom segments. In addition, diagonal shear damage is also developed in the bottom segment (Segment 1). The non-retrofitted column collapses at Impact 05 with the impact velocity 3.59m/s. In comparison, much less damages are found on the FRP-wrapped column, S5KD-FRP-BJ. FRP rupture can be observed at the edge of the bottom segment due to excessive hoop stress as well as the direct impact load. No other damage occurs to the rest of the column. After the seven impacts in the test, the column still survives (not

collapsed) although the residual displacement at the top of the column is large as shown in the Figure.

a) S5KD-FRP-BJ b) S5KD-BJ

Figure 9 Comparison of damage and failure of columns under bottom segmental joint impact a) FRP retrofitted column; b) Non-retrofitted column

3.2.3 Impact load time histories

Figure 10a shows the impact load time histories of column S5KD-FRP-BJ. The impact load time histories show typical dual-peaks because of the interaction between the impactor and the segmental column. The peak loads increase as impactor velocity increases except for Impact 07 whose peak load is smaller (46kN). This is because of the damage of the column in previous impacts that makes the column less stiff. Nevertheless, the loading duration steadily increases indicating the impact acting on the column for longer duration. Comparing the recorded impact load time histories between the retrofitted and non-retrofitted columns in Figure 10b, it can be found that the impact load on the two columns are very similar. When subjected to 0.67m/s impact in Impact 02, a peak impact load of 20.5kN is measured on column S5KD-BJ while that on column S5KD-FRP-BJ is 19.4kN. The duration of the both loading time histories are about 25ms. Similarly, when subjected to 1.37m/s impact, the peak impact loads are both about 35kN and the load duration about 30ms. These results imply wrapping the concrete segments with FRP has insignificant effects on the column stiffness therefore the interaction

between the impactor and the two columns are similar. When the columns are subjected to 2.71m/s impact, noticeably lower 2nd peak load (28kN) can be found on the non-retrofitted column S5KD-BJ, while that on column S5KD-FRP-BJ is about 42kN. The impact load duration for the former column is 44ms and the latter is less than 40ms. The difference is because the high initial peak impact load damages the concrete segment of the non-retrofitted column. The degradation of the stiffness of the column due to damages of the segment results in the lower 2nd peak in the load time history but longer loading duration.

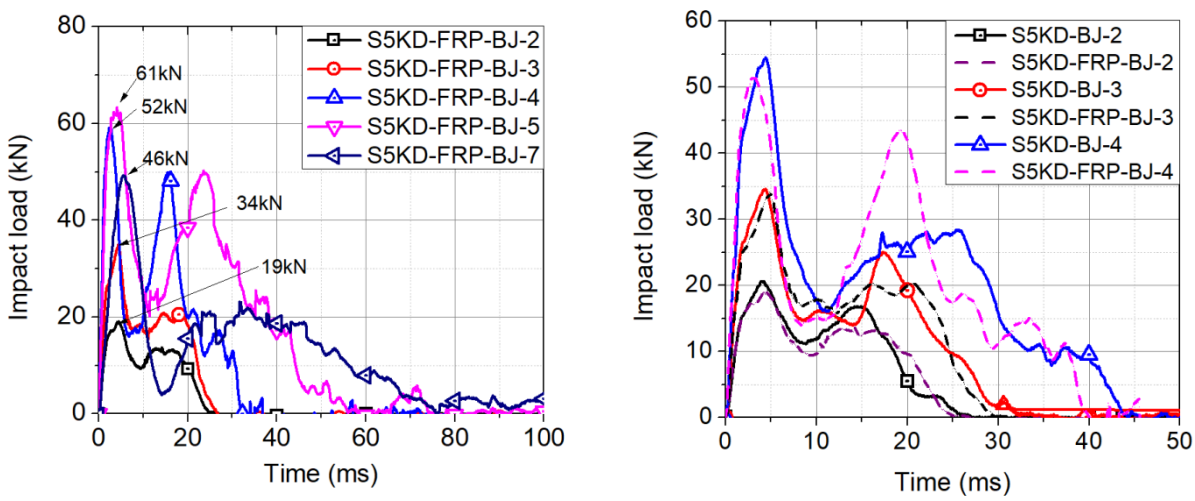

a) b)

Figure 10 Impact load time histories for a) S5KD-FRP-BJ; b) comparison with S5KD-BJ

3.2.4 Deflection time histories

Figure 11a shows the deflection time histories of column S5KD-FRP-BJ at the impacted segmental joint. Unlike those recorded when impacted at mid-span, as shown in Figure 11a the deflection is featured with an initial peak associated with the forced vibration phase followed by a series of small amplitude fast oscillations till the column comes to complete rest. As joint opening initiates under high velocity impacts in Impact 05, 06 and 07, larger initial peak deflections are resulted. Also because of segmental joint opening, the vibration period of the column becomes longer.

Figure 11b compares the deflection time histories at the impacted segmental joints of the retrofitted and non-retrofitted columns. As can be seen, the FRP wrapped column has

smaller deflections. For instance, when subjected to 0.67m/s impact (Impact 02), slightly smaller peak deflection (2.1mm) is measured on column S5KD-FRP-BJ comparing to 2.9mm peak deflection measured on column S5KD-BJ. And almost no residual deflection is found on the former column while nearly 2mm residual deflection is found on the non-retrofitted column. When subject to 3.59m/s impact (Impact 05), 30mm peak deflection is recorded on the retrofitted column S5KD-FRP-BJ, compared to 34mm peak deflection on the non-retrofitted column.

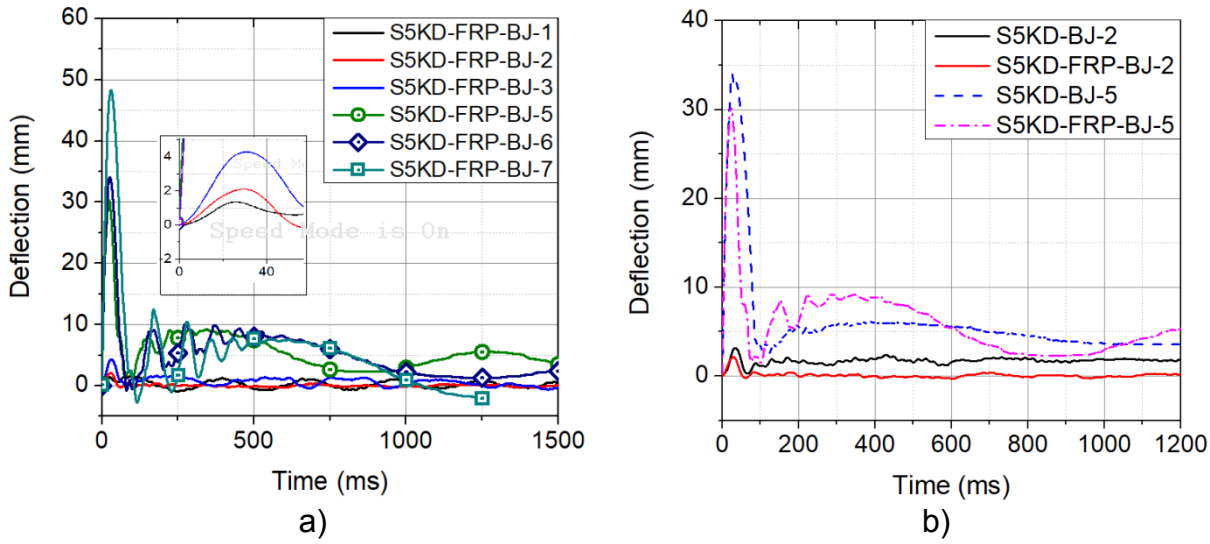

Figure 11 Deflection time histories at bottom segmental joint for a) column S5KD-FRP-BJ; b) comparison with column S5KD-BJ

The peak and residual displacements at the top of the two columns are summarized and plotted against the imposed impulse in Figure 12a. As shown, retrofitted column always has lower peak deflections than the non-retrofitted column. For example, when subjected to 0.67m/s impact (about 250kN-ms impulse), a peak deflection of 3.9mm is measured on column S5KD-FRP-BJ, which is 13% less than that of column S5KD-BJ. When the impact velocity is 1.37m/s (about 500kN-ms impulse), the retrofitted column deforms with a peak deflection of 12mm at the top of the column while that of the non-retrofitted column is nearly 16mm. The difference is mainly because of the higher flexural stiffness of the retrofitted column compared to the non-retrofitted column with lower stiffness owing to damages to the concrete segments. Nevertheless, the difference on the residual displacement at the top of the two columns are not as significant as the peak

deflection. For instance, in Impact 03 similar residual displacements (about 4.6mm) are measured on the two columns. After Impact 04, larger residual displacement (7mm) is found on column S5KD-FRP-BJ as compared to 4.5mm on column S5KD-BJ. More apparent difference can be found on relative displacement. As shown in Figure 12b, about 2mm relative displacement is measured between Segment 1 and 2 of the non-retrofitted column after Impact 03 (about 500kN-ms) which further increases to 4.7mm in Impact 04. The relative displacement is mainly because of the shear crack in the base segment of the non-retrofitted column. In comparison, no relative displacement is found between the bottom two segments until Impact 06 (about 1600kN-ms impulse) that only less than 1mm relative displacement is found. This is because the FRP wrap substantially improved the shear resistance of the concrete segment.

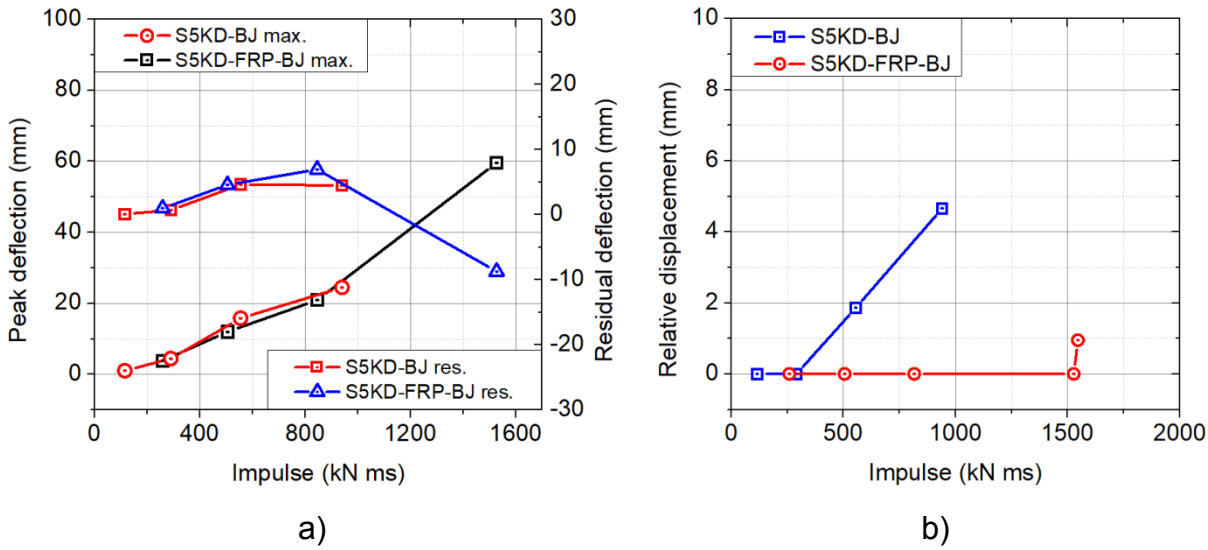

a) b)

Figure 12 Comparison of a) peak and residual deflections at column top; b) relative displacement between Segment 1 and 2

3.3 Impact at bottom segment

3.3.1 Deformation-to-failure process

Figure 13 shows the high-speed camera images of column S5KD-FRP-BS when it was impacted at the centre of the bottom segment (Impact 04 and 05). Because the impact location is very close to the base of the column but not at the segmental joint, no flexural bending response is generated. Instead, as shown in Impact 04, the impactor

pushes the bottom segment to move sideways at t=10ms. Because of inertia resistance from the top added mass, the top part of the segmental column primarily remains at its original location. The column experiences large deformation at the bottom segment but manages to maintain its stability. In Impact 05, under the substantial lateral impact force apparent larger lateral displacement is resulted in the bottom segment. Because of the confinement of the FRP wrap, no obvious damage can be observed to the concrete segment. Slight twisting can be observed between Segment 2 and 3, indicating the low torsion resistance provided by the smooth dome shear key. The column collapses eventually as a result of the excessive drift of the bottom segment.

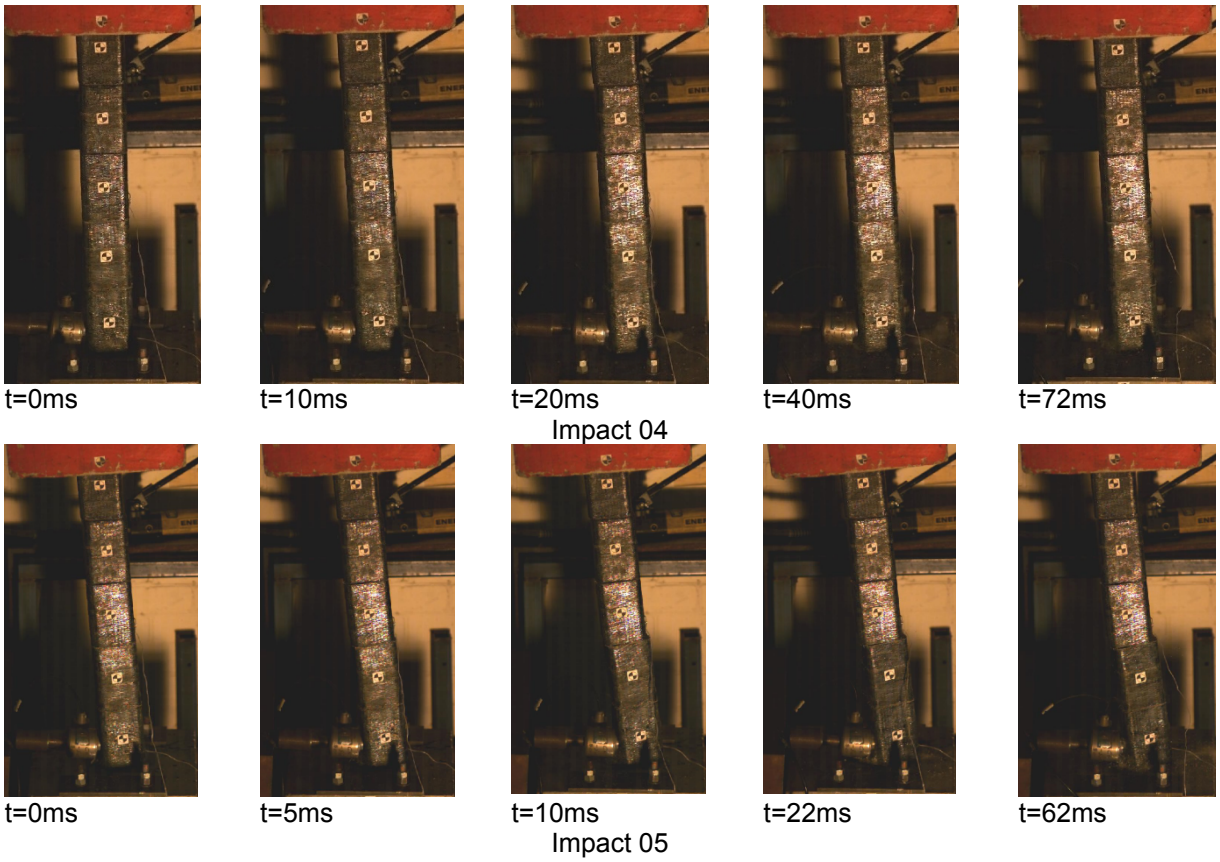

Figure 13 High-speed camera images of the responses of column S5KD-FRP-BS

3.3.2 Damage and failure of the column

Figure 14 compares the damage and failure modes of the column. It is apparent that on the non-retrofitted column the substantial lateral impact force smashes the bottom concrete segment with severely deformation to the reinforcing cage and the starter bars.

In comparison, when retrofitted with FRP wrap, the bottom segment is pushed by the large impact force and the column eventually collapses but no apparent damage to the bottom segment can be observed. Because of excessive deformation, FRP rupture occurs in the bottom segment. Moreover, one of the starter bars is severely bent and the other one is totally sheared off, indicating the bottom segment experiences very large lateral movement.

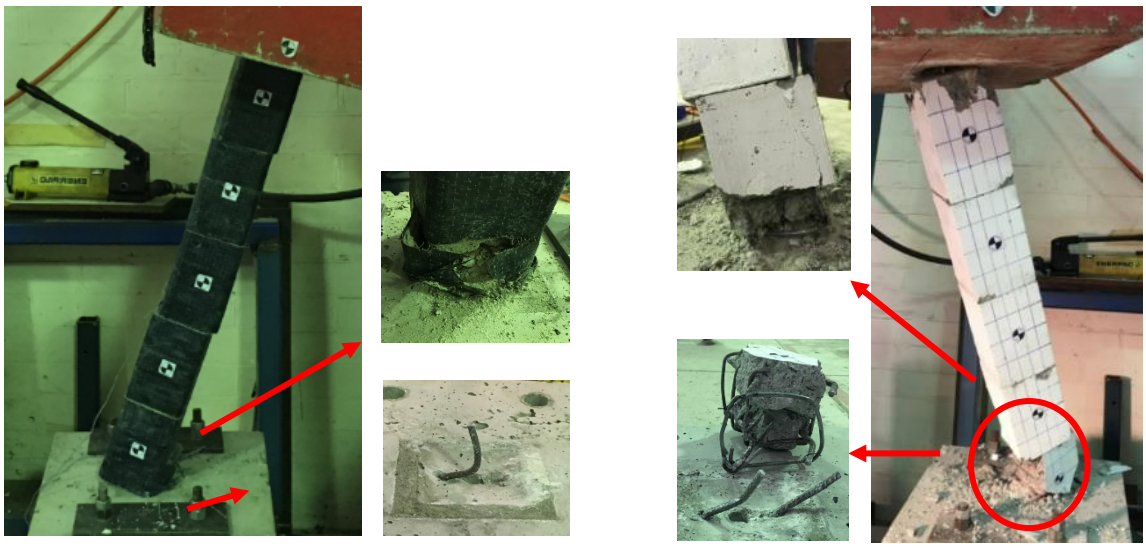

a) S5KD-FRP-BS b) S5KD-BS

Figure 14 Comparison of damage and failure modes of columns under bottom segmental impact a) FRP-retrofitted column; b) Non-retrofitted column

3.3.3 Impact time histories

The impact load time histories recorded on column S5KD-FRP-BS are shown in Figure 15a. It can be found that as impact velocity increases, the peak impact load also increases. For instance, in Impact 01 a peak load of 16.5kN is measured which increases to about 24kN in Impact 02. A peak load of 48kN is recorded in Impact 03 which quickly reduces to about 21kN and followed by a second peak of about 34kN before dissipates to zero. As the integrity of the column degrades due to column accumulated damage, the peak load in Impact 04 does not further increase but the loading duration becomes longer. Figure 15b compares the impact load time histories for the two columns with and without FRP retrofit when subjected to base segment impact. As can be seen, very similar peak impact loads are recorded for the two columns. This is because the initial peak load is

governed by the inertia resistance and local stiffness of the column. As damage accumulated in the non-retrofitted column, smaller peak load is resulted in Impact 04 (about 43kN) comparing to 48kN on the FRP-wrapped column. The impactor also acts longer on the latter column, about 50ms comparing to 36ms in the retrofitted column.

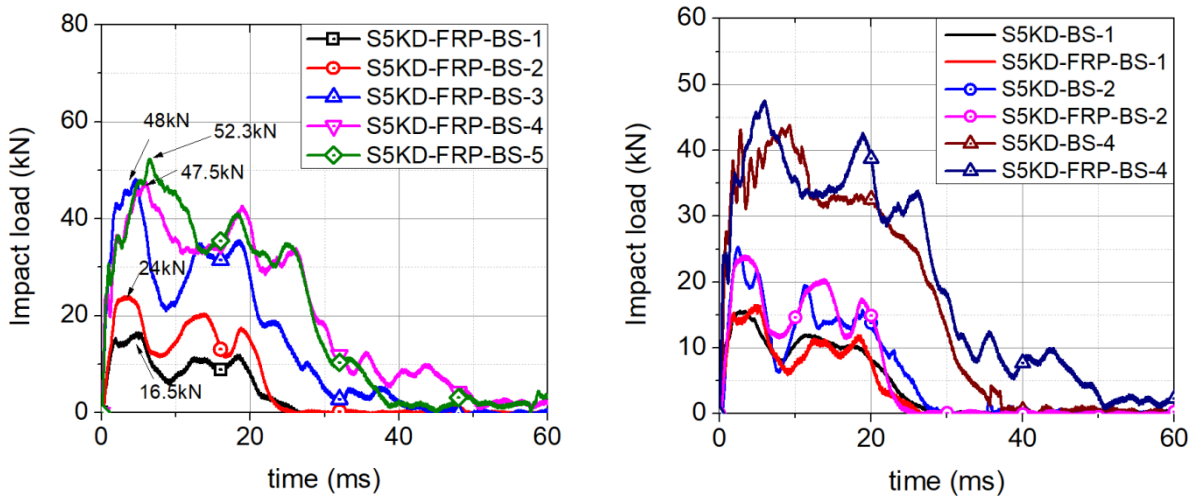

a) b)

Figure 15 Impact load time histories for a) S5KD-FRP-BS; b) comparisons with S5KD-BS

3.3.4 Deflection time histories

Figure 16a shows the deflection time histories recorded at the centre of the bottom segment (Segment 1). Because the impact load does not generate any flexural bending in the column but mainly direct lateral movement in the bottom segment, the deformation time histories measured on the bottom segment follow primarily the impact loading history, however they do not return to zero, but to the respective residual displacement. As impact level increases, the maximum and residual displacement at the bottom segmental also increase. For instance, in Impact 01 a peak deflection of 2.6mm is resulted, which increases to 11.7mm and 29.7mm in Impact 03 and 04. The corresponding residual displacement increases from zero to about 5mm and 17mm. Figure 16b compares the deflection time histories at the centres of the bottom segments for the retrofitted and non-retrofitted columns. It can be found that similar peak and residual deflections are recorded in low velocity impact (Impact 01). When impact velocity is higher (in Impact 04), a

maximum deflection of about 29.7mm is recorded on the retrofitted column while that on the non-retrofitted column is only 24.8mm. This is because the FRP wrapped column is relatively intact and the impactor could force the entire segment to move horizontally, while in comparison the non-retrofitted segment experiences direct shear damage. The impact kinetic energy is dissipated through the damage of the column. It is evidenced that larger residual displacement (19.4mm) is found on the non-retrofitted column while that on the retrofitted column is less than 17mm.

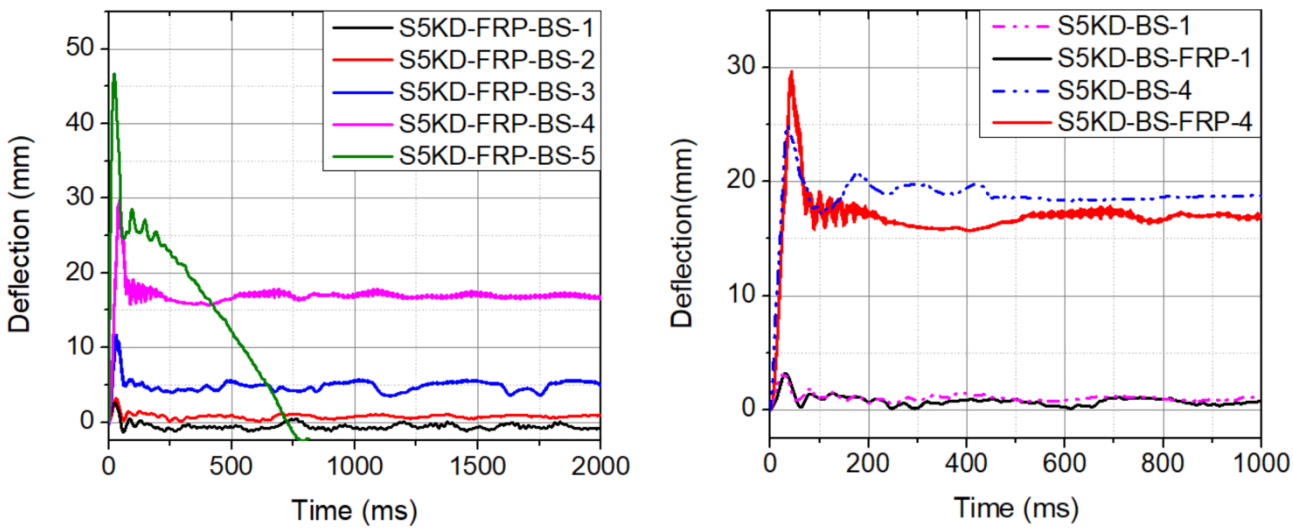

a) b)

Figure 16 Deflection time histories at the centre of Segment 1 for a) S5KD-FRP-BS; b) comparison with column S5KD-BS

Figure 17a summarizes the peak and residual displacements at the centre of the bottom segment of the retrofitted and non-retrofitted columns. It can be found that very similar peak and residual deflections are recorded on the two columns when the impact levels are small in Impact 01 and 02. As impact level increases, concrete damage occurs in the non-retrofitted column, while no obvious damage is observed in the FRP wrapped segment although it experiences higher peak deflections. For example, a peak deflection of 11.7mm is found on column S5KD-FRP-BS in Impact 03, while that on column S5KD-BS is only 7.8mm. In Impact 04, the peak deflection in the retrofitted column is nearly 30mm. In comparison, only 25mm peak deflection is recorded on the non-retrofitted column. The non-retrofitted column has smaller deformation because of intensive

concrete damage, which absorbs significant amount of impact energy and also makes the segment softer, hence smaller deformation as compared to the retrofitted column. Nevertheless, most of the deflections of the retrofitted column recovers after the impact by the posttensioning bars. After Impact 04, only 16.8mm residual deflection is measured on column S5KD-FRP-BS, whereas 19.4mm residual deflection is found on the non-retrofitted column. Therefore, it can be found that applying FRP wrap to segmental column could effectively reduce concrete damage when subjected to direct impact on the bottom segment; however, larger peak deflection but lower residual displacement could be expected.

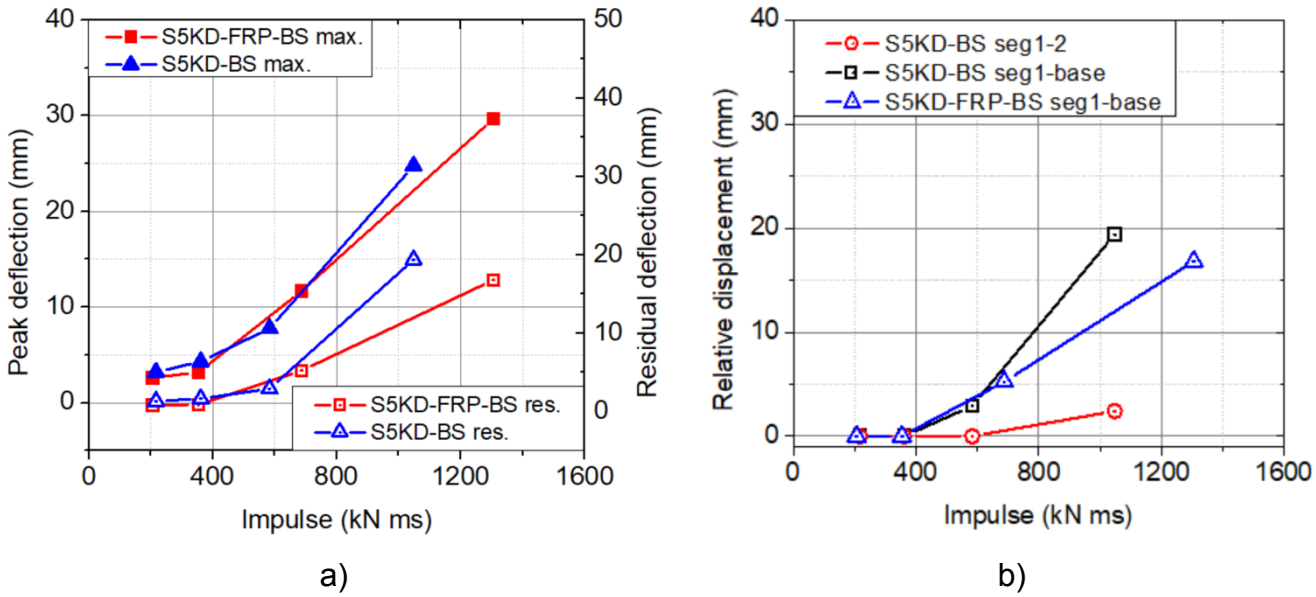

Figure 17 Comparison of a) peak and residual deflections at centre of bottom segment; b) relative displacement

Since the segmental column mainly shows direct shear response, relative displacement between adjacent segments could be a major concern. Figure 17b compares the segmental displacement between the retrofitted and non-retrofitted columns. It can be seen that relative displacements begin to occur in Impact 03. Slightly larger relative displacement (5.3mm) is found on the retrofitted column in comparison to 2.9mm for the non-retrofitted column. As discussed above, this is because the FRP wrapped segment is intact and forced to move laterally. When the columns suffer major damage in Impact 04, nearly 20mm relative displacement is found on the non-retrofitted column while that on the retrofitted column is less than 17mm. Also, with FRP wrap less

shear key damage occurs on the retrofitted column. As a result, only minimum relative displacement is observed between Segment 1 and 2 on the retrofitted column, whereas about 3mm is found on the non-retrofitted column.

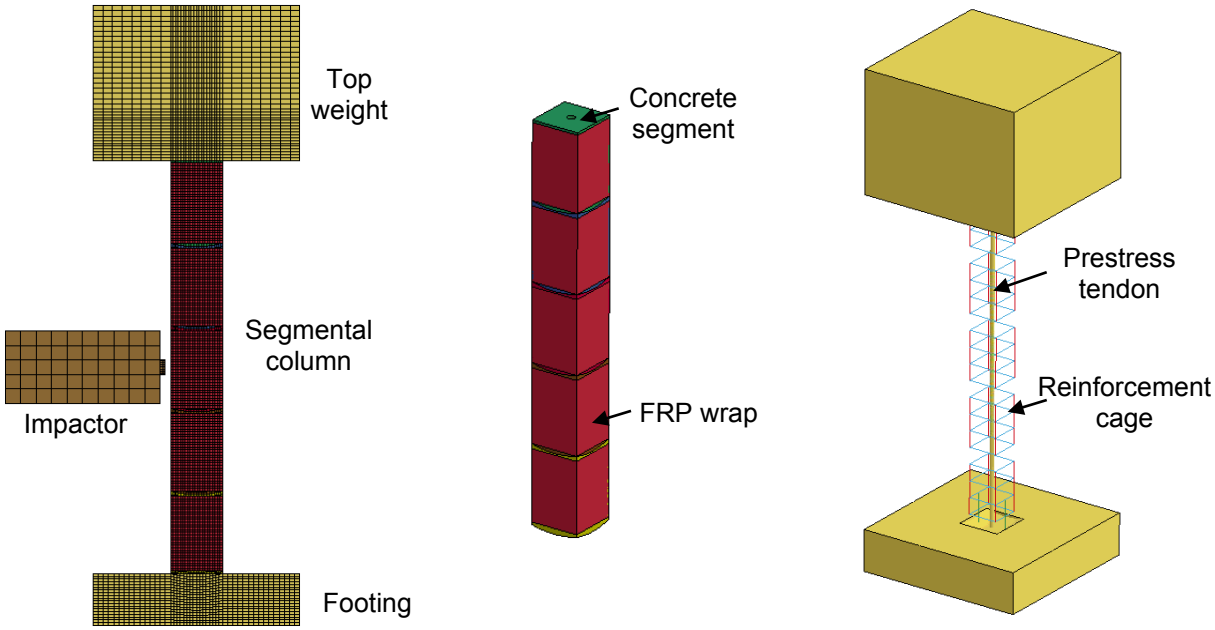

Figure 18 Numerical model of segmental column under impact

4. Numerical Modelling

A detailed three-dimensional model of the segmental column is generated to replicate the above-mentioned laboratory impact tests. The columns are subjected to gradually increased impact velocities. The responses of the columns from the numerical simulation are compared with the lab testing results to validate the numerical model. The concrete damage status, FRP strain and damage status in the numerical model are used to help better understand the performance of the FRP retrofitted segmental columns under lateral impact loads.

4.1 Model details

Numerical modeling is carried out using commercial software LS-DYNA [28] which is a popularly used hydro-code. Figure 18 depicts the numerical model of the segmental column, where SOLID_164 solid element (8-node constant stress) with single integration

point is adopted for concrete and prestress tendon, BEAM_161 beam element (3-node) with 2 by 2 gauss integration for steel reinforcement, and Belytschko-Tsay shell for FRP. 5mm mesh is selected for the numerical model after mesh sensitivity analysis. To ensure conservation of mass and energy no erosion is used in the numerical model. The contact between concrete segments is modelled with Automatic_Surface_To_Surface contact element with empirical static and dynamic friction coefficient of 0.6 and 0.5, respectively. The contact between the prestress tendon and the concrete segments are also modelled with Automatic_Surface_To_Surface contact but without consideration of friction effect. The post-tensioning force in the tendon is initiated through dynamic relaxation with implicit analysis prior to the explicit dynamic analysis for impact. Perfect bond is assumed by merging the nodes together between the FRP wrap and the concrete segments.

4.2 Material models

For concrete material Concrete_Damage_REL3 (MAT72) is selected in this study. MAT72 model is one of the most popularly used material models for concrete material in dynamic analysis. It is a plasticity-based model which considers confining pressure, strain rate effect and concrete damage. In MAT72 model, the stress tensor is expressed as the sum of the hydrostatic stress and the deviatoric stress. The hydrostatic stress varies with concrete volume, and the deviatoric stress controls the shape deformation. The EOS_TABULATED_COMPACTION model in LS-DYNA is used to correlate the pressure as a function of the volumetric strain. As illustrated in Figure 19, three shear failure surfaces are employed to depict the intact, yield and residual strength curves of concrete material. The deviatoric stress remains elastic during the initial loading and reloading phase until the stress reaches the initial yield surface. The deviatoric stress then increases until the maximum strength surface is reached. The response can be perfectly plastic or softens to the residual strength surface beyond this stage. A damage scalar is used to account for concrete damage, which ranges from 0 to 1.0 for concrete material experiencing strain hardening, and from 1.0 to 2.0 for material softening stage.

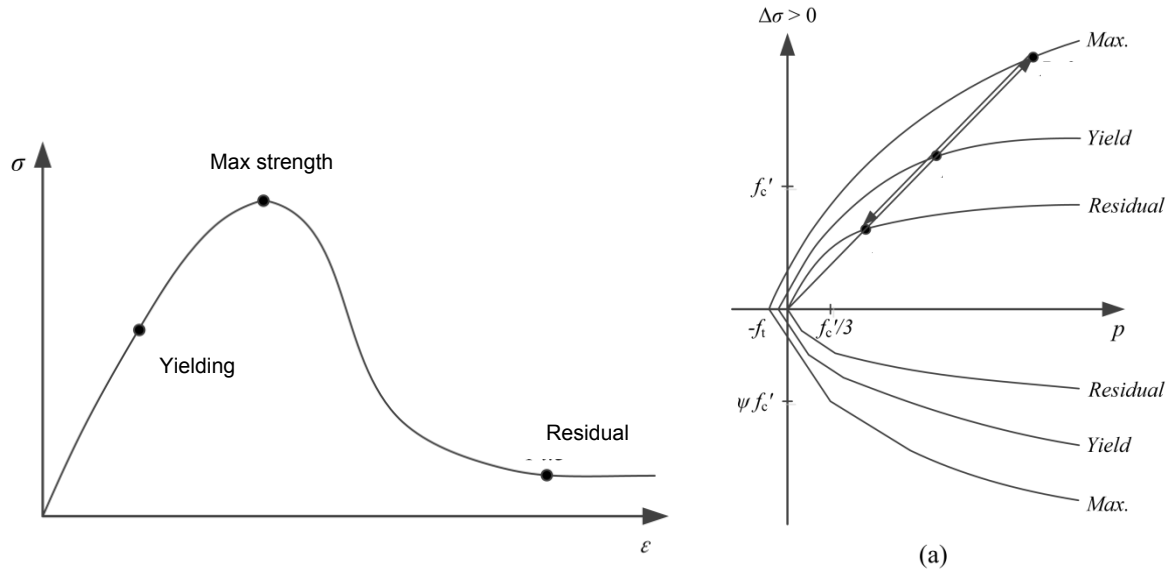

a) Stress-strain curve b) Meridian of strength surfaces

Figure 19 K&C MAT72 concrete material model

Dynamic increase effect has been widely recognized to influence material dynamic properties. With experimental and numerical studies, relation of dynamic increase factor (DIF) with respect to strain rate are available for concrete [29-31]. Equations for the DIF of concrete material for both compressive and tensile strength are defined as:

$$\text{CDIF} = f_{cd}/f_{cs} = 0.0419(\log\dot{\varepsilon}_d)+1.2165 \quad \text{for } \dot{\varepsilon}_d \leq 30\text{s}^{-1} \tag{1}$$

$$\text{CDIF} = f_{cd}/f_{cs} = 0.8988(\log\dot{\varepsilon}_d) - 2.8255(\log\dot{\varepsilon}_d) + 3.4907 \quad \text{for } \dot{\varepsilon}_d > 30\text{s}^{-1} \tag{2}$$

$$\text{TDIF} = f_{td}/f_{ts} = 0.26(\log\dot{\varepsilon}_d) + 2.06 \quad \text{for } \dot{\varepsilon}_d \leq 1\text{s}^{-1} \tag{3}$$

$$\text{TDIF} = f_{td}/f_{ts} = 2(\log\dot{\varepsilon}_d) + 2.06 \quad \text{for } 1\text{s}^{-1} < \dot{\varepsilon}_d \leq 150\text{s}^{-1} \tag{4}$$

where f_{cd} and f_{td} are the dynamic compressive and tensile strengths at the strain rate $\dot{\varepsilon}_d$, f_{cs} and f_{ts} are the static compressive and tensile strengths at strain rate of 10^{-6}s^{-1}.

The prestress tendon and reinforcement including both longitudinal rebar and tie are modelled with Piecewise_Linear_Plasticity model (MAT_24). The advantage of this model is that it enables arbitrary stress-strain curve and strain rate dependency to be defined. For simplicity, a bi-linear elastic-plastic relation is utilized. The yield strength, ultimate strength, Young's modulus and tangential modulus follow the material properties

of those used in the experiment. Table 2 summarizes the parameters of material models in the current study. The DIF equation for reinforcement used in the study is defined as [32],

$$\text{DIF} = \left(\frac{\dot{\varepsilon}}{10^{-4}}\right)^{\alpha} \tag{5}$$

where for the yield stress $\alpha = \alpha_{fy} = 0.074 - 0.04 f_y/414$; and for the ultimate stress, $\alpha = \alpha_{fu} = 0.019 - 0.009 f_y/414$, in which f_y is the yield strength of the reinforcement.

Plastic_Kinematic model (MAT_003) is used to model the unidirectional FRP wraps. The FRP wraps are simplified as an isotropic and elastic material without defining the kinematic hardening plasticity. The tensile strength, failure strain and elastic modulus are 1640MPa, 0.02 and 78GPa. The strain rate effect is neglected because the expected strain rate under impact loading in this study is relatively low. Previous study [33] has proved that such simplification gives acceptable prediction.

The steel impactor is modelled with a linear elastic material model (MAT_001) since no plastic deformation is resulted. The density is 7800kg/m^3 and Young's modulus is 200GPa.

Table 2 Summary of material properties for rebar and prestress tendon

Material		Value	Unit
Longitudinal rebar	Density	7800	kg/m^3
	Yield stress	500	MPa
	Young's modulus	200	GPa
	Poisson's ratio	0.3	
Stirup	Density	7800	kg/m^3
	Yield stress	300	MPa
	Young's modulus	200	GPa
	Poisson's ratio	0.3	
Prestress tendon	Density	7800	kg/m^3
	Yield stress	1860	MPa
	Young's modulus	208	GPa
	Poisson's ratio	0.3	
FRP wrap	Density	2500	kg/m^3
	Young's modulus	78	GPa

Failure strain	0.02

4.3 Model validation

4.3.1 Mid-span impact

Figure 20a compares selected central deflection time histories from the numerical simulations and the lab test. It can be found that when subjected to low speed impact (0.64m/s in Impact 02), numerical model gives very close prediction of deflection time histories of the lab test. When subjected to 2.62m/s impact, a peak central deflection of 66mm is predicted by the numerical model which is also close to that in the lab test. When subjected to 3.72m/s impact (in Impact 05), a peak deflection of 122mm is predicted by the numerical model which is slightly higher than that in the lab test (117mm), and less rebound is predicted which could be due to lower residual concrete strength in the KC concrete model.

Figure 21a shows the damage contour of the deformed column when subjected to mid-span impact. As can be observed when subjected to 3.72m/s impact the numerical model could closely predict the deformation shape of the lab tested column and captures the joint opening between Segment 3 and 4. As compared in Figure 22a, FRP rupture on Segment 3 and Segment 1 are also predicted by the numerical simulation. With the numerical model, concrete damage, which is difficult to be directly observed in the test owing to the FRP wrap, can be assessed. As shown in Figure 21a, concrete damage occurs around the segmental joint at the mid span and the base of the column due to flexural bending. Because of the effective confinement of FRP wrap, the damage to concrete segments is insignificant. As impact velocity increases, more severe concrete damages occur and spread to more segmental joints owing to less effective FRP confinement to the concrete segments at the joints.

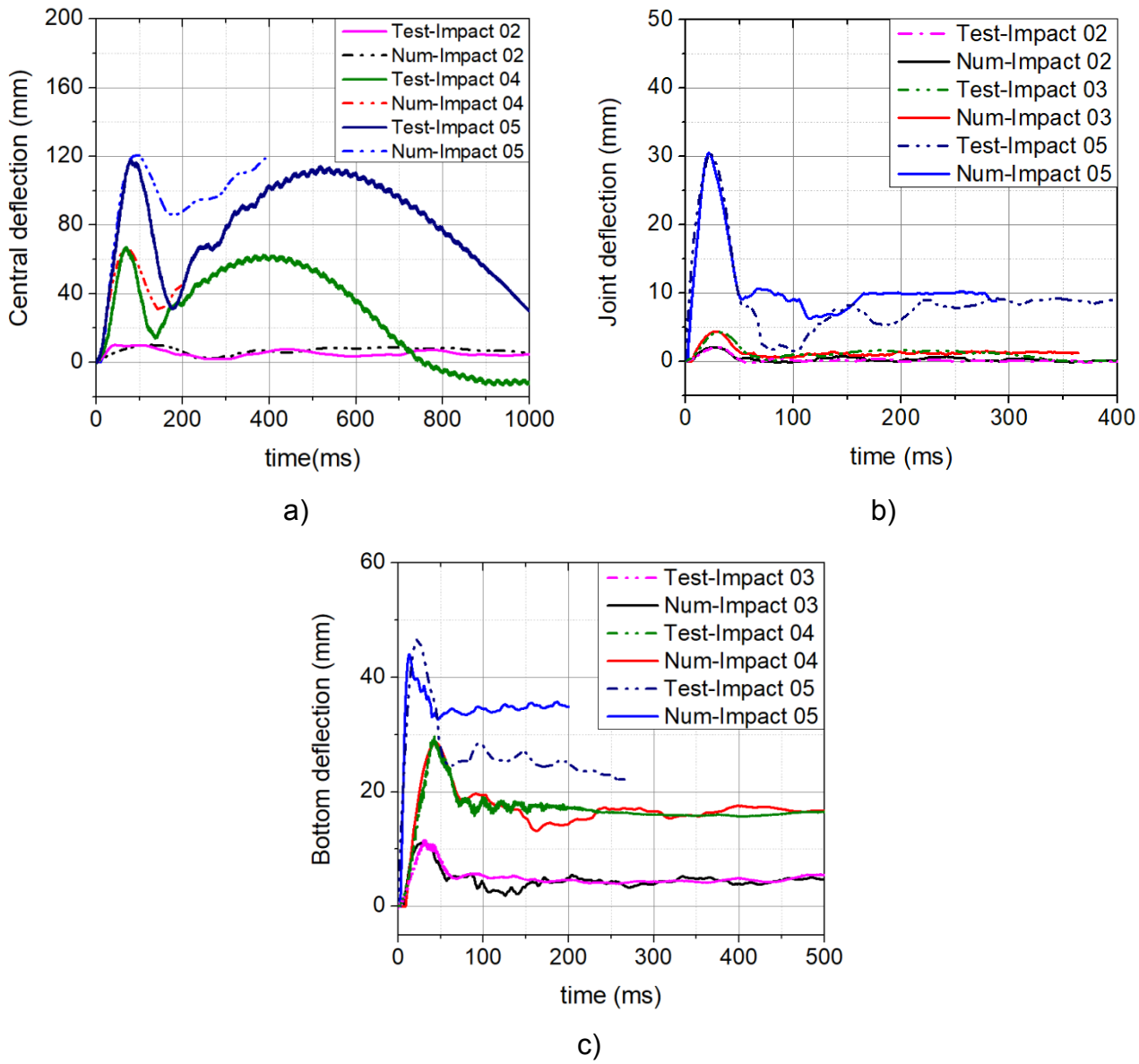

Figure 20 Comparison of deflection time histories a) mid span deflection when impacted at the mid span; b) bottom segmental joint when impacted at the bottom segmental joint; c) centre of bottom segment when impacted at the base segment

4.3.2 Impact at the bottom segmental joint

Figure 20b compares the deflection time histories at the segmental joint under the impact. A close match of the deflections from the numerical modelling and the lab test can be found when subjected to 0.64m/s and 1.38m/s impacts in Impact 02 and 03. When subjected to 3.72m/s impact, a peak central deflection of 32mm is predicted by the numerical model which is slightly larger than 30mm in the lab test. The forced vibration of

the column can be very well reproduced by the numerical model, however because of the difficulty in exactly modelling the concrete residual strength, the free vibration response in the numerical model differs from that of the laboratory test. Nevertheless, similar level of residual deflections is found. Figure 21b compares the response of the column and shows the concrete damage contour. As can be observed, segmental joint opening between Segment 1 and 2 is modelled numerically which is very similar to that in the lab testing when the columns are subjected to 3.72m/s impact. The overall deformation mode of the column from the numerical simulation matches closely with that in the experimental test. From the concrete damage contours, it can also be found that with FRP confinement almost no concrete damage is resulted when subjected to low velocity impact (0.64m/s). Because of flexural bending at the bottom segmental joint between Segment 1 and 2, minor concrete compressive damage occurs. Also because of the large shear force transferred through Segment 1, the concrete shear key in connection with footing suffers damage. As impact velocity increases, more column damage is developed. For instance, when subjected to 3.72m/s impact concrete damage extends from left side of the cross section due to flexural compression to the entire shear key region, indicating large shear forces being born by the column. Nevertheless, the rest parts of the wrapped concrete segments are mostly intact indicating the effectiveness of the FRP wrapping. Figure 22b shows the principal strain contour on the FRP wrap. It can be seen that FRP rupture occurs at the top edges of Segment 1 which matches with the lab observation. This is because of the excessive compressive stress at the segmental joint due to flexural bending deformation. Large strain is also developed on the FRP wrap. In addition, Minor FRP damage is also found at the corner of Segment 4 and 5 at the top of segmental joint. This confirms the flexural deformation mode of the column when subjected to impact at bottom segmental joint that results in joint opening at the impact point. The damage moves upwards as the local vibration mode during forced-vibration phase changes to the global vibration mode during free-vibration phase. A large curvature is formed at the top segmental joint near the supported mass.

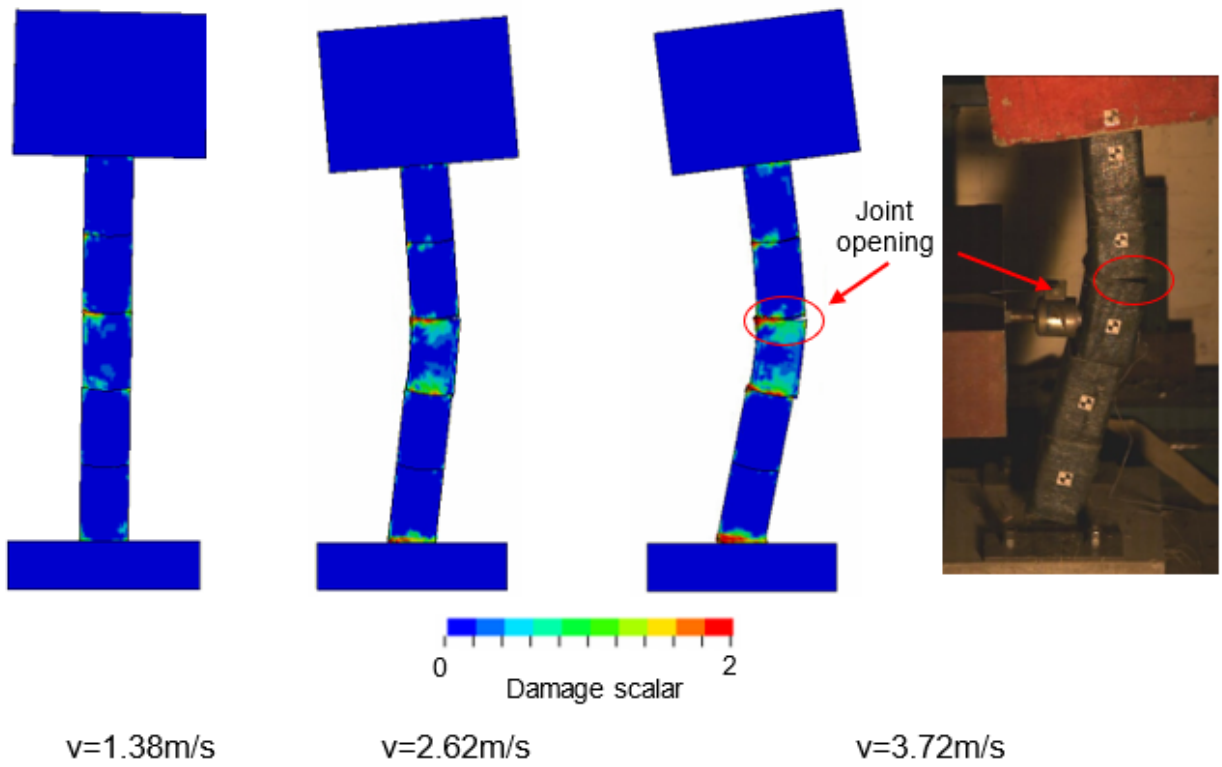
Joint
opening
0
2
Damage scalar
v=1.38m/s
v=2.62m/s
v=3.72m/s

a)

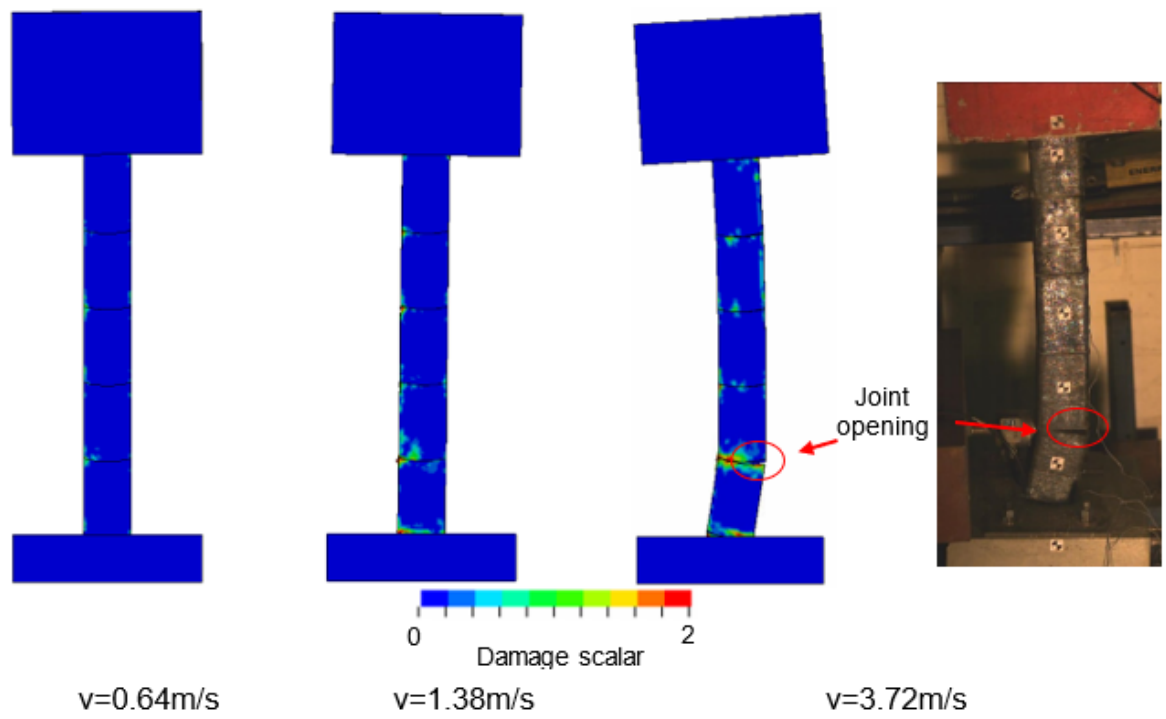
Joint
opening
0
2
Damage scalar
v=0.64m/s
v=1.38m/s
v=3.72m/s

b)

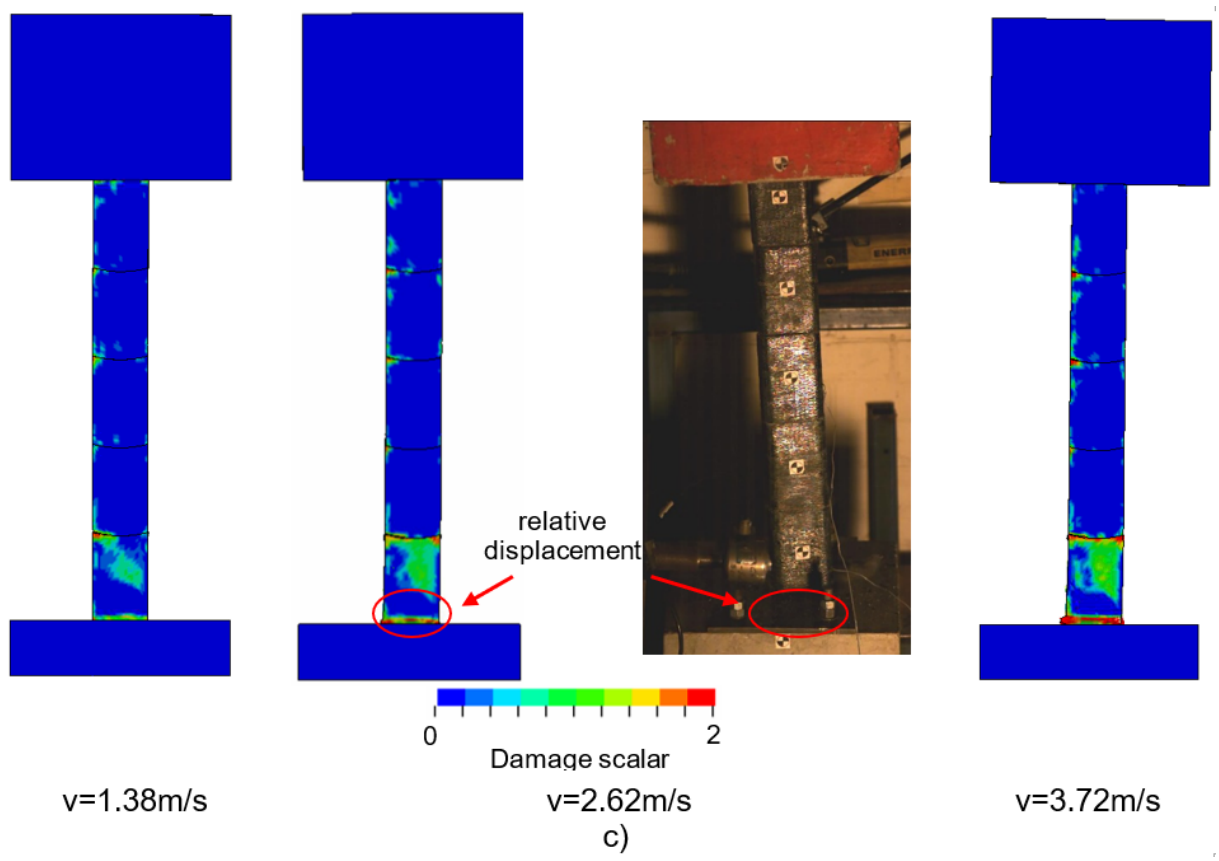

Figure 21 Concrete damage contours: a) mid-span impact; b) bottom segmental joint impact; c) base segment impact

4.3.3 Impact at the bottom segment

Figure 20c compares the deflection time histories at the centre of the bottom segment under the impact. It can be found that the deflection time histories from the numerical simulation agree well with the experimental results in Impact 03 and 04. Both the peak and the residual deflections match closely. When the column is subjected to the ultimate 3.72m/s impact, slightly smaller peak deflection is predicted by the numerical model (about 44mm) in comparison to 47mm peak deflection as measured in the laboratory test. The residual displacement in the numerical model is also larger. This is again probably because of the difficulty in accurately modelling the residual strength of the concrete material in the adopted numerical model. Nevertheless, the behavior of the column is still in general reasonably well modelled with the numerical method.

Figure 21c compares the response of the numerical model and the lab tested column. Because the concrete shear key of Segment 1 connecting the footing is severely damaged under the lateral impact induced shear force, large relative movement is developed as depicted in the images. In the numerical model, severe concrete damage at the shear key is also modelled, but no erosion is applied to the concrete elements in the numerical model to ensure mass and energy conservation. From the concrete damage contours shown in Figure 21c, it can be observed that concrete damages are developed and accumulated primarily in the bottom segment (Segment 1) due to the direct impact induced large shear forces, which transfers through the shear key to the footing. Because limited flexural bending deformation is developed in the segmental column, almost no damage occurs to the above concrete segments. Diagonal shear damage can be observed in Segment 1 from numerical simulation. Figure 22c shows the strain contour in the FRP. As can be observed, large strain is developed in the FRP wrap confining the bottom concrete segment. A small FRP rupture is predicted in the numerical simulation which replicates that being observed in the lab test on Segment 1. This indicates that despite the segmental column primarily experiences direct shear vibration mode when subjected to bottom segment impact, after the shear key accumulates damages, the entire column rotates against the bottom left corner which leads to large compressive stress at the corner of Segment 1, resulting in FRP rupture.

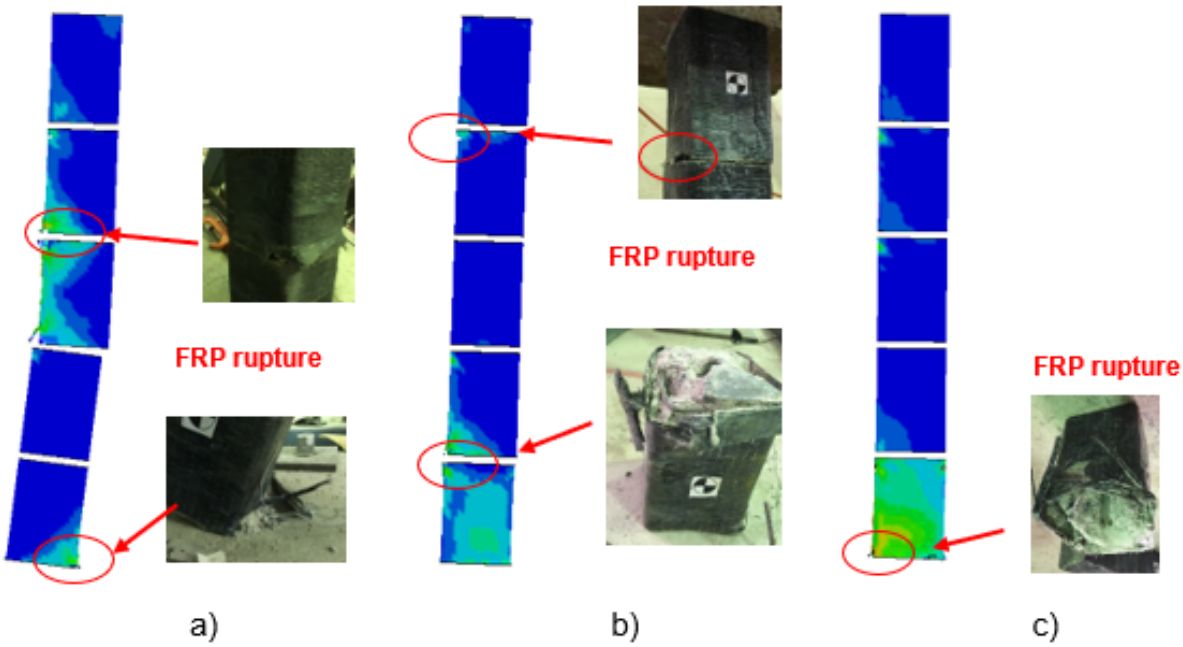

Figure 22 Principal strain contour in the FRP wrap when subjected to a) mid-span impact; b) bottom segmental joint impact; c) bottom segment impact

Figure 22 Principal strain contour in the FRP wrap when subjected to a) mid-span impact; b) bottom segmental joint impact; c) bottom segment impact

5. Conclusion

This paper presents experimental and numerical studies to investigate the performance of segmental column retrofitted with FRP wrap when subjected to lateral impact loading. The columns are impacted at mid-span which excites the flexural bending deformation mode; at bottom segmental joint which excites the combined flexural bending and shear deformation mode; and directly at bottom concrete segment which leads to direct shear failure mode. It is found that with FRP wrap the impact resistance performances of the column are improved when it is subjected to mid-span impact and bottom segmental joint impact. This is because the FRP wrap provides effective confinement which improves concrete ultimate compressive strength and residual strength, and therefore leads to less column damage. When the column is subjected to the bottom segment impact, FRP wrap limits the damage to the bottom concrete segment. However, when subjected to high velocity impact, damage shifts down to the shear key connecting the segmental column

to the footing. More severe damage occurs and consequentially leads to larger column lateral displacement. The developed numerical model yields good predictions of the column with FRP wrapped segments. The model can be used in the analysis and design of segmental columns subjected to lateral impact loads.

Acknowledgement

The authors would like to acknowledge the financial support from Australian Research Council for this project.

Reference

[1] M. Shahawy, Prefabricated Bridge Elements and Systems to limit traffic disruption during construction, Transportation Research Board, 2003.

[2] J.T. Hewes, M.N. Priestley, Seismic design and performance of precast concrete segmental bridge columns, 2002.

[3] S.L. Billington, J. Yoon, Cyclic response of unbonded posttensioned precast columns with ductile fiber-reinforced concrete, Journal of Bridge Engineering, 9 (2004) 353-363.

[4] C.C. Chou, Y.C. Chen, Cyclic tests of post-tensioned precast CFT segmental bridge columns with unbonded strands, Earthquake engineering & structural dynamics, 35 (2006) 159-175.

[5] T. Arai, Y. Hishiki, K. Suda, Y. T., S. Takizawa, T. Onabe, KaTRI Annual Rep. No. Vol. 48, Development of a new precast segmental PC pier, Kajima Corporation, Tokyo, Japan, 2000.

[6] K.C. Chang, C.H. Loh, H.S. Chiu, J.S. Hwang, C.B. Cheng, J.C. Wang, Seismic behavior of precast segmental bridge columns and design methodology for applications in Taiwan, Taiwan Area National Expressway Engineering Bureau, Taiwan, 2002.

[7] C. Li, H. Hao, X. Zhang, K. Bi, Experimental study of precast segmental columns with unbonded tendons under cyclic loading, Advances in Structural Engineering, 21 (2018) 319-334.

[8] Y.C. Ou, M.S. Tsai, K.C. Chang, G.C. Lee, Cyclic behavior of precast segmental concrete bridge columns with high performance or conventional steel reinforcing bars as energy dissipation bars, Earthquake engineering & structural dynamics, 39 (2010) 1181-1198.

[9] Y.-C. Ou, P.-H. Wang, M.-S. Tsai, K.-C. Chang, G.C. Lee, Large-scale experimental study of precast segmental unbonded posttensioned concrete bridge columns for seismic regions, Journal of structural engineering, 136 (2009) 255-264.

[10] X. Zhang, H. Hao, C. Li, Multi-hazard resistance capacity of precast segmental columns under impact and cyclic loading, International Journal of Protective Structures, 9 (2018) 24-43.

[11] X. Zhang, C. Li, H. Hao, Performance of prefabricated segmental columns under impact loading, in: Proceedings of 4th International Conference on Protective Structures (ICPS4), Beijing, China, 2016.

[12] X. Zhang, H. Hao, C. Li, Experimental investigation of the response of precast segmental columns subjected to impact loading, International Journal of Impact Engineering, 95 (2016) 105-124.
[13] X. Zhang, H. Hao, C. Li, The effect of concrete shear key on the performance of segmental columns subjected to impact loading, Advances in Structural Engineering, (2016) 1369433216650210.
[14] X. Zhang, H. Hao, C. Li, T.V. Do, The behavior of precast segmental column with domed shear key and unbonded post-tensioning tendon under impact loading, in press with Engineering Structures, (2018).
[15] Y.-C. Ou, M. Chiewanichakorn, A.J. Aref, G.C. Lee, Seismic performance of segmental precast unbonded posttensioned concrete bridge columns, Journal of structural engineering, 133 (2007) 1636-1647.
[16] S. Motaref, M.S. Saiidi, D. Sanders, Shake table studies of energy-dissipating segmental bridge columns, Journal of Bridge Engineering, 19 (2013) 186-199.
[17] J.H. Shan, R. Chen, W.X. Zhang, Y. Xiao, W.J. Yi, F.Y. Lu, Behavior of Concrete Filled Tubes and Confined Concrete Filled Tubes under High Speed Impact, Advances in Structural Engineering, 10 (2007) 209-218.
[18] X. Yan, S. Yali, Impact Behaviors of CFT and CFRP Confined CFT Stub Columns, Journal of Composites for Construction, 16 (2012) 662-670.
[19] B. Scott, R. Park, M. Priestley, Stress-strain behavior of concrete confined by overlapping hoops at low and high strain rates, in: Proceedings of Journal Proceedings, 1982.
[20] A. Mirmiran, M. Shahawy, M. Samaan, H.E. Echary, J.C. Mastrapa, O. Pico, Effect of column parameters on FRP-confined concrete, Journal of Composites for construction, 2 (1998) 175-185.
[21] S. Pessiki, K.A. Harries, J.T. Kestner, R. Sause, J.M. Ricles, Axial behavior of reinforced concrete columns confined with FRP jackets, Journal of Composites for Construction, 5 (2001) 237-245.
[22] P. Rochette, P. Labossiere, Axial testing of rectangular column models confined with composites, Journal of Composites for Construction, 4 (2000) 129-136.
[23] Y.C. Wang, J.I. Restrepo, Investigation of concentrically loaded reinforced concrete columns confined with glass fiber-reinforced polymer jackets, Structural Journal, 98 (2001) 377-385.
[24] L. Lam, J. Teng, Design-oriented stress–strain model for FRP-confined concrete, Construction and building materials, 17 (2003) 471-489.
[25] ACI 440, Guide for the design and construction of externally bonded FRP systems for strengthening cocrete structures., ACI Committee, 2002.
[26] J.B. Mander, M.J. Priestley, R. Park, Theoretical stress-strain model for confined concrete, Journal of structural engineering, 114 (1988) 1804-1826.
[27] H. Hao, W. Chen, X. Zhang, Dynamic Tensile Properties of Carbon and Basalt Fibre Reinforced Polymer Materials, 8th International Conference on Fibre-Reinforced Polymer (FRP) Composites in Civil Engineering, Hongkong, 2016.
[28] LS-DYNA Keyword User's Manual, Volume, I Version 971 Livermore Software Technology Corporation, 2007.

[29] Y. Hao, H. Hao, X. Zhang, Numerical analysis of concrete material properties at high strain rate under direct tension, International Journal of Impact Engineering, 39 (2012) 51-62.
[30] L.J. Malvar, J.E. Crawford, Dynamic increase factors for concrete, Naval Facilities Engineering Service Center Port hueneme CA, 1998.
[31] H. Hao, Y. Hao, J. Li, W. Chen, Review of the current practices in blast-resistant analysis and design of concrete structures, Advances in Structural Engineering, 19 (2016) 1193-1223.
[32] L.J. Malvar, J.E. Crawford, Dynamic increase factors for steel reinforcing bars [C], in: Proceedings of 28th DDESB Seminar. Orlando, USA, 1998.
[33] Z. Li, L. Chen, Q. Fang, W. Chen, H. Hao, Y. Zhang, Experimental and numerical study of basalt fiber reinforced polymer strip strengthened autoclaved aerated concrete masonry walls under vented gas explosions, Engineering Structures, 152 (2017) 901-919.